CNIC-00922
CNDC-0015
INDC(CPR)-033 / L

中国核科技报告

CHINA NUCLEAR SCIENCE & TECHNOLOGY REPORT

COMMUNICATION OF NUCLEAR DATA PROGRESS

No. 12 (1994)

Chinese Nuclear Data Center

VOL 27 No 01 Beijing, December, 1994

中国核情报中心
China Nuclear Information Centre

CNIC-00922
CNDC-0015
INDC(CPR)-033 / L

COMMUNICATION OF NUCLEAR DATA PROGRESS

No. 12 (1994)

Chinese Nuclear Data Center

China Nuclear Information Centre

Atomic Energy Press

Beijing, December, 1994

EDITORIAL NOTE

This is the twelfth issue of *Communication of Nuclear Data Progress* (CNDP), in which the achievements in nuclear data field since the last year in P. R. China are carried. It includes the measurements of neutron multiplication in Pb; theoretical calculations on isomeric state cross sections in neutron radiative capture for ^{59}Co, ^{103}Rh and on n+^{235}U, ^{239,240}Pu reactions, a comparison of the maximum entropy method of analysis with the exciton model plus the master equation, a processing code system searching for optimal neutron optical potential parameters, the pre– and post–management of code DWUCK4, a code for supplement of gamma production data to evaluated neutron data; the update and modification of the total cross sections for S, K, Ti, Zr, Sb, Hf, Pb, and evaluation of ^{197}Au(n,2n)^{196}Au reaction cross section from threshold to 80 MeV; a fast reactor multigroup constant library CL50G, benchmark testing of total cross section for Fe, O, Na, N, a data processing and critical safety analyzing code system NJOY–WIMS; atomic mass and discrete level schemes sublibraries; comparison of two approximation methods to deal with PPP phenomenon in practice; an evaluated data library for light particle reflections from solid surfaces, study of physical sputtering systematics.

We hope that our readers and colleagues will not spare their comments, in order to improve the publication.

Please write to Drs. Liu Tingjin and Zhuang Youxiang
Mailing Address : Chinese Nuclear Data Center
China Institute of Atomic Energy
P. O. Box 275 (41), Beijing 102413
People's Republic of China
Telephone : 86–1–9357729 or 9357830
Telex : 222373 IAE CN
Facsimile : 86–1–935 7008
E–mail : CIAEDNP@ BEPC 2

CONTENTS

I EXPERIMENTAL MEASUREMENT

Measurement of Neutron Multiplication in Pb by Mn Foils

Chen Yuan Liu Rong Guo Haiping
Jiang Wenmian Shen Jian

(Southwest Institute of Nuclear Physics and Chemistry, Chengdu)

Abstract

The Leakage neutron multiplication in bulk lead has been measured using the total absorption detector and relative method. The polyethylene sphere of 138 cm in diameter is used as the moderator and total absorption detector. The measured results from ^{55}Mn foils and ^{6}Li glass are compared. The neutron multiplication is 1.74 with the lead shell of 23.1 cm thick. The measured result is consistent with the calculated one with ANISN code and ENDF / B-6 evaluated data within the experimental error.

Introduction

It is widely considered that lead is the same good material as beryllium used to multiply neutron in blanket of fusion reactor. However, the measurements for neutron multiplication focus on Be in the past years, because people generally emphasized beryllium material and there was a large difference between experimental and calculated results for beryllium. Up to now only a few laboratories[1~3] have carried out the experiments of neutron multiplication in Pb, and there are a large differences among measured results. The measured results are 10% larger than the calculated ones. To clarify the inconsistency, it is very necessary to carry out the experiments of neutron multiplication in Pb. We made a set of lead samples of five thicknesses. The maximum thickness is 23.1 cm which is 6 mm thicker than Kurchatov's lead sample. The experiments have

been performed for a set of lead samples using ^{6}Li detectors. To obtain more reliable results, Mn foils were used to measure multiplication in lead of 23.1 cm thick. The results from Mn foils and ^{6}Li detectors are compared.

1 Experimental Method

The leakage neutron multiplications are measured by the total absorption detector (TAD) and relative method. Neutrons leaking from the lead sample are sufficiently moderated in polyethylene. The neutrons, except those with small portion leaking out of moderator, are fully absorbed by hydrogen in moderator. Absorption of ^{6}Li, ^{55}Mn and H to slow neutrons conforms to the $1/v$ law. Therefore ^{6}Li and ^{55}Mn detectors are used to imitate absorption of H to slow neutrons. The apparent and true multiplications are

$$M_a = {}^{m}H_A / {}^{o}H_A = {}^{m}Mn_A / {}^{o}Mn_A \qquad (1)$$

and

$$M_L = M_a \ (\ 1 - {}^{o}X_A - {}^{o}L \ ) \ + \ {}^{m}X_A \ + \ {}^{m}L \ + \ \mathrm{Pb(n,x)} \qquad (2)$$

where M_a : apparent multiplication

M_L : true multiplication

m and o : with and without sample

H_A : absorption of H to neutrons in TAD

X_A : nonhydrogen absorption in moderator

L : the leakage out of moderator

Pb(n,x) : lead absorption of neutrons reflected by moderator into lead sample

X_A, L and Pb(n,x) are calculated. Every term mentioned above is normalized to one source neutron, and integrated over the whole sphere.

2 Experimental Setup

2.1 Total Absorption Detector

The total absorption detector is a high-density polyethylene sphere, as shown in Fig. 1. Its inner and outer diameters are 46 and 138 cm, respectively. There are a target chamber channel and five measuring channels in the equatorial plane of TAD being the direction of 0°, 40°, 80°, 120° and 150° to D^{+} beam line.

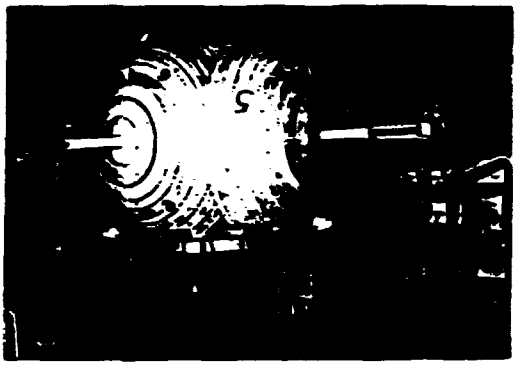

Fig. 1 Total absorption detector

2.2 Lead Sample

The lead sample is composed of two hemisphere shell with 4 cm in inner diameter and 50.2 cm in outer diameter. There is a target chamber channel with 3 cm in diameter in the interface. The purity of lead is larger than 99.9% . The impacts on the measured value from the little impurity is negligible.

2.3 Target Chamber

The target chamber is made from aluminum and composed of the wide and thin parts. The thin one is 28 cm in length, 2.6 cm in diameter and 1 mm in wall thickness. The wide one is 60 cm in length, 9.4 cm in diameter and 2 mm in wall thickness. The α–particle monitor is in the direction of 178.5° to D^+ beam line. The fraction of D–D neutrons in D–T neutrons is less than 1% . The stability of neutron source is better than 2% . The target surface is cooled by compressed air.

2.4 Activation Foils

Mn foils are alloy of Mn and Ni contained 20% Mn. The size of Mn foils is 13.6 and 15 mm in diameter. Their thicknesses are 1 mm. Mn foils are put in small polyethylene chambers well manufactured, as shown in Fig. 2. The nineteen foils are put in the chambers together. The first foil is located at the inner surface of moderator. The interval among foils is 1 cm from foil 1 to foil 9, 2 cm from foil 9 to foil 13, 3 cm from foil 13 to foil 16, 5 cm from foil 16 to foil 19.

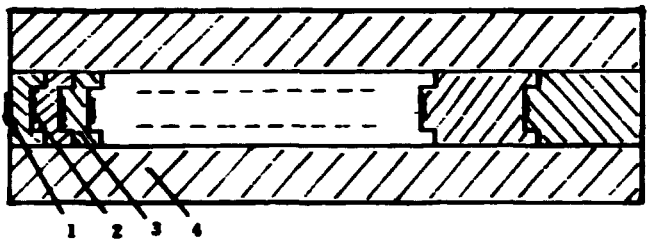

Fig. 2 Activation foil detectors

1, 2 activation foils; 3 small polyethylene chamber; 4 polyethylene sleeve.

2.5 Irradiation and Measurement

Activation foil detectors were put in the direction of 80° in moderator and continuously irradiated for 8.5 h. The neutron flux is about 1×10^9 n / s. The integrated counts of associated alpha particles to monitor neutron field were recorded once each 500 s. As soon as the irradiation was stopped, the γ activity of ^{56}Mn was measured by the high purity germaniuum (HPGe) detector. The HPGe detector is shielded by lead. The natural background counts were 3 per minute, subtracted from the measured γ activity of ^{56}Mn. The measuring conditions with and without sample were kept the same.

3 Data Processing

When stopping time is t_0, γ activity of i–th foil is :

$$N_i^0(t_0) = \frac{N_i \lambda}{e^{-\lambda(t_1 - t_0)} - e^{-\lambda(t_2 - t_0)}} \tag{3}$$

After normalized with associated alpha particles and weight, γ activity is :

$$N_i(t_0) = \frac{N_i(t_0)}{M_i F_a} \tag{4}$$

It is related to the neutron number (unit volume) in the position, in TAD, at which a foil is located.

$$F_a = \sum_{K=1}^{N} \rho a K \, e^{-(N-K) T_a \lambda} \tag{5}$$

The symbols in the relations (3) to (5) mean :

λ : decay constant of ^{56}Mn.

N_i : the measured γ activity of the i–th foil in t_2-t_1 period.

M_i : weight of the i–th foil.

F_a : alpha normalizing factor weighted.

N : the number of times of recorded alpha particles during irradiated period.

K : the K–th record in N.

T_a : time to record alpha particles once.

P_{aK} : counts of alpha particles in T_a period of the K–th record.

The spatial distribution of neutron density in TAD is integrated according to the relation below :

$$N=\frac{4\pi}{3}\sum_{i=1}^{n}\frac{[\,N_i(t_0)+N_{i+1}(t_0)\,]}{2}(r_{i+1}^3-r_i^3) \qquad (6)$$

where r is the distance between a foil place and the center of TAD.

4 Results and Discussion

After the γ counts of a foil in t_2-t_1 period had been measured, in terms of relation (3) γ intensity in stopping time was obtained. Then in terms of relation (4) γ intensity unit mass and per alpha particle was obtained. The radial distribution of γ activity measured in the direction of 80° to D^+ beam line is shown in Fig. 3. Fig. 4 is the radial distribution of neutron count rate of ^{6}Li glass detector under the same condition.

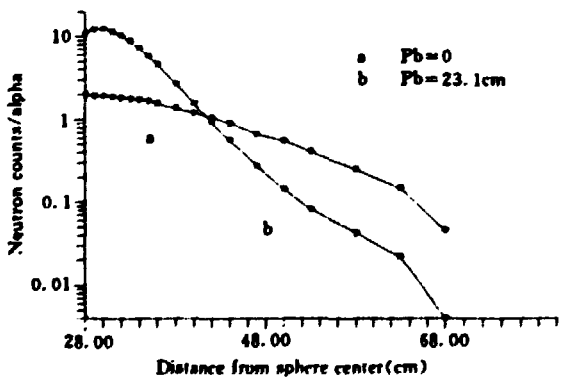

Fig. 3 Neutron distribution obtained by ^{56}Mn activity

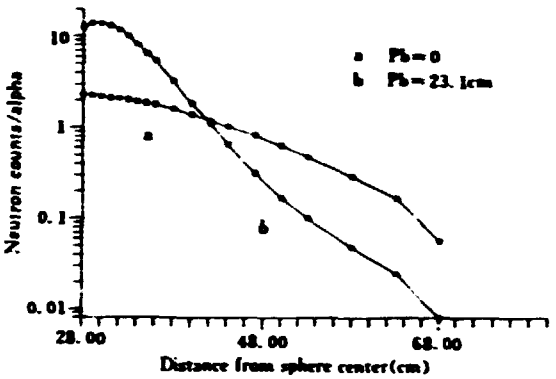

Fig. 4 Neutron distribution measured by ^{6}Li glass detector

The corrections in relation (2) are calculated using 1-D ANISN code and ENDF / B-6 library data. The calculating condition of ANISN is that the number of energy group is 30, P_3 and S_{16}, the low threshold 10^{-4} eV, and the energy of source neutrons 13.5~ 14.9 MeV. The energy and flux distributions of source neutron are isotropic. The calculated results are listed in Table 1.

The apparent multiplications from ^{55}Mn foils and ^{6}Li glass are listed in Table 2. The true multiplication in bare lead is obtained from relation (2). The measured and calculated multiplications in bare lead are listed in Table 3.

Table 1 The corrections

Pb Thickness (cm)	Nonhydrogen absorption	Leakage	Reflection
0	0.0592	0.1085	--
2.0 / 25.1	0.0152	0.0131	0.1462

Table 2 Apparent multiplications

Pb Thickness (cm)	Measurement		Calculation
	^{55}Mn	^{6}Li	
2.0 / 25.1	1.884	1.887	1.880

Table 3 Multiplication in bare lead

Pb Thickness (cm)	Experiment		Calculation	E / C
	^{55}Mn	^{6}Li		
2.0 / 25.1	1.743	1.745	1.735	1.006

From Table 3, the results from two detectors have a good consistency. It indicates that the measured leakage multiplication is independent of thermal neutron cross section of the detector, provided that the detector conforms well to the $1/v$ law. The measured result is consistent with the calculated one with ANISN code and ENDF / B–6 data.

5 Conclusions

The experimental errors of measuring multiplication from ^{6}Li glass and ^{55}Mn foils are 2.8% and 3.2%, respectively. Because of the less counts of the ^{56}Mn activity, especially nearby the edge of moderator, the error from Mn foils is slightly larger than that from the ^{6}Li detector. If the neutron intensity and γ counting time are increased, the statistical error may be decreased. The results obtained from two detectors of different thermal neutron cross section are consistent within the experimental error. The measured and calculated results are also consistent within the experimental error.

The work is supported by the National Science Foundation of China and the Science Foundation of CAEP.

References

[1] S. I. Bessonov et al., IAE–5453 / 11, Moscow, (1992)

[2] T. Elfruth et al., Atomkernenergie Kerntechnik, 49, 121(1987)

[3] A. Takahashi et al., Proc. 12th Symp. Fusion Technology, Julich, FRG. Sep. 13～17, 1982, p. 687, IAEA (1983)

[4] Y. Chen et al., Fusion Technology, 23, 68(1993)

[5] Y. Chen et al., "Measurement of Neutron Multiplication in Bulk Lead", to be published

[6] Y. Chen et al., Fusion Technology, 19, 1919(1991)

[7] D. F. Tian, "Calculated Corrections of Multiplication Measurement in Lead", private communication

CN 150 1853

II THEORETICAL CALCULATION

Isomeric State Cross Sections in the Neutron Radiative Capture

Zhang Xizhi Liu Jianfeng Zhang Guohui

(Department of Physics, Zhengzhou University, Zhengzhou)

The integral equations describing the cascade γ deexcitation processes are provided to calculate the ground state and the isomeric state cross sections in the neutron radiative capture. In the initial conditions, the contributions of the pre-equilibrium and the primary γ transitions after statistical equilibrium are considered simultaneously. The numerical calculations have been done for ^{59}Co and ^{103}Rh in the neutron incident energy region between 0.1 and 3 MeV. The calculation results are compared with those of the experiments and some simple discussions are presented.

Introduction

The study on the neutron radiative capture is important both in theory and in practical use. It is indispensable for the determination of the lower excited energy level characteristics and the higher excited energy level wave functions of the nucleus, and for the tests of nuclear reaction models as well as the theoretical calculations of the nuclear data. For over last 30 years, a lot of studies on the mechanism of the neutron radiative capture has been done. Firstly, on the basis of the compound nucleus statistical theory, some non-statistical effects [1, 2] were presented. Owing to the success of the exciton model in describing pre-equilibrium particle emissions, this model was also used to describe pre-equilibrium gamma emission processes. A fairly successful case was the pre-equilibrium exciton phonon coupling model[3]. Secondly, the angular momentum and parity conservation relation to the exciton model was introduced in order to research pre-equilibrium gamma emissions[4]. This model may give

some more clear physical interpretations for the main non-statistical effects. Since the built calculation formulas of the non-statistical processes are all used in practical calculation, they are still important both in theory and in practical use. Recent years, further study on the statistical theory of the compound nucleus is developed, the main work of which is focused on the photon strength functions[5].

The purpose of this paper is to research the calculation method of the ground state and the isomeric state cross sections in the neutron radiative capture on the basis of the work mentioned above. It is necessary to meet the development of the nuclear data work requirement for cross section branch ratio of isomertic state, and to meet the nowadays plenty of experimental data of the isomeric state cross sections accumulated. By comparing the calculated results with experiments, further tests can be done for the presented mechanism of the radiative capture as well as for some related theories.

I Calculation formulas

Since the pre-equilibrium γ emissions correspond to the higher energy photons and the final states are some lower excited states, it can be assumed that the system reaches the statistical equilibrium state after a pre-equilibrium photon emits. For the convenience of description, a set of integral equations is given which can be used to describe the cascade γ deexcited process of the nucleus in statistical equilibrium states, and regard the excitons of the primary γ transition of compound system to each level as initial condition.

Suppose that E_m is the highest excitation energy of $A+1$ nucleus formed by the neutron bombarding the target nucleus A, E_m to E_c is the continuous region of the energy levels, $\rho(E, J, \pi)$ is the level density of the continuous region, E, J, π represent the energy, spin and parity respectively. Below E_c, there are N discrete levels including the ground state denoted by (E_1, J_1, π_1), (E_2, J_2, π_2) $\cdots$ (E_N, J_N, π_N), among which the k-th level ($1 < k \leqslant N$) is a isomeric state. The function $\sigma_c(E, J, \pi)$ means that $\sigma_c(E, J, \pi)\,dE$ represents the total excitation cross section of the levels with spin J, prity π and energy between E and $E+dE$ in the whole transition process and $\sigma_{c_0}(E,J,\pi)$ is its initial value. σ_i is the total excitation cross section of ith discrete level in the whole process and σ_{i_0} is its initial value. Then the whole cascade γ deexcitation process can be solved by the following integral equations.

$$\begin{cases} \sigma_e(E,J,\pi) = \sigma_{e0}(E,J,\pi) + \int_{E_e}^{E_m} \sum_{J'\pi'} \sigma_e(E',J',\pi') \dfrac{\Gamma_{\gamma,EJ\pi}^{E'J'\pi'}}{\Gamma^{E'J'\pi'}} \rho\ (E,J,\pi)\ \mathrm{d}E' & (1) \\ \sigma_j = \sigma_{j0} + \sum_{i=j+1,\ i\neq k}^{N} \sigma_i S^{ij} + \int_{E_j}^{E_m} \sum_{J'\pi'} \sigma_e\ (E',J'\pi') \dfrac{\Gamma_{\gamma j}^{E'J'\pi'}}{\Gamma^{E'J'\pi'}}\ \mathrm{d}E', \\ (\ j\ =\ 1,\ 2,\ \cdots,\ N\ ) & (2) \end{cases}$$

where $\Gamma^{E'J'\pi'}$ is the total width of the level $E'J'\pi'$, $\Gamma_{\gamma}^{E'J'\pi'}$ is γ partial width, S^{ij} is the gamma transition branching ratio between discrete levels. σ_{j0} and $\sigma_{e0}(E, J, \pi)$ consist of two terms as below

$$\sigma_{j0} = \sigma_{j0}^{\mathrm{PEQ}} + \sigma_{j0}^{\mathrm{EQ}} \tag{3}$$

$$\sigma_{e0}(\ E,J,\pi\ ) = \sigma_{e0}^{\mathrm{PEQ}}(\ E,J,\pi\ ) + \sigma_{e0}^{\mathrm{EQ}}(\ E,J,\pi\ ) \tag{4}$$

where the one with indices PEQ represent the contribution of the pre-equilibrium γ emission, the one with EQ represent the contribution of the equilibrium γ emission[6]. By solving integral Eqs. (1) and (2), the cross sections of the neutron radiative capture of the ground state and isomeric state can be obtained, which take the form of

$$\sigma_{n\gamma s} = \sigma_1 = \sigma_{10} + \sum_{i=2,\ i\neq k}^{N} \sigma_i S^{i1} + \int_{E_1}^{E_m} \sigma_e(E',J',\pi) \frac{\Gamma_{\gamma 1}^{E'J'\pi'}}{\Gamma^{E'J'\pi'}}\ \mathrm{d}E' \tag{5}$$

$$\sigma_{n\gamma m} = \sigma_k = \sigma_{k0} + \sum_{i=k+1}^{N} \sigma_i S^{ik} + \int_{E_k}^{E_m} \sigma_e(\ E',J',\pi\ ) \frac{\Gamma_{\gamma k}^{E'J'\pi'}}{\Gamma^{E'J'\pi'}}\ \mathrm{d}E' \tag{6}$$

it is obvious that the total radiative capture cross section $\sigma_{n\gamma}$ can be read as

$$\sigma_{n\gamma} = \sum_{j=1}^{N} \sigma_{j0} + \int_{E_1}^{E_m} \sum_{J'\pi'} \sigma_{e0}\ (\ E',J',\pi'\ )\ \rho\ (\ E',J',\pi\ )\ \mathrm{d}E' = \sigma_{n\gamma s} + \sigma_{n\gamma m} \tag{7}$$

II Calculation Results and Discussion

By using of the scheme mentioned above, the numerical calculations have been made for ^{59}Co and ^{103}Rh in the neutron incident energy region between

0.1 and 3 MeV. The calculated results are compared with experimental data[7]. In the calculation, Becchetti–Greenless' optical potential [8], and Gilbert–Gameron's energy level density formulas[9] are used. The optical potential parameters were adjusted to make the calculated total cross section and the elastic scattering cross section fit the experimental data. Choosing the level density parameters makes that the calculated result of the low excited level accumulation number roughly agrees with the experimental data, and it is adjusted again in the calculating radiative capture cross section. γ partial widths are calculated by using giant dipole resonance model. For the resonance parameters, the experimental value[10] is adopted. This paper takes no account of M1, E2 or more multipole transitions because of the following reasons : (1) the calculated results show that these transition values are far less than E_1[5]; (2) the experimental values of these parameters of transition are still short at present, only the existing adjustable parameters are inducted; (3) for the γ transition branch ratio among discrete levels, the experimental values are adopted, in which multipole transition contribution is included.

The calculated results of radiative capture cross section $\sigma_{n\gamma}$ for ^{59}Co, and comparison with experimental data are shown in Fig. 1. The calculated results of isomeric state (i. e. ^{60m}Co, $E=0.0585$ MeV, $J^\pi=2^+$) cross section and comparison with experimental data are shown in Fig. 2. Fig. 3 shows the calculated results of the ground state cross section $\sigma_{n\gamma g}$ (curve a) and isomeric state cross section $\sigma_{n\gamma m}$ (curve b) for ^{103}Rh (i. e. ^{104m}Rh, $E=0.129$ MeV, $J^\pi=5^+$) and comparison with experimental data. From Figs. 1 ~ 3, it can be concluded that the calculated results are in good agreement with experimental values both in quantity and energy changing tendency although a little discrepancy exists. This discrepancy can be interpreted as the following reasons :

(a) The difference between ground state and isomeric state is little in the energy, but large in the angular momentum. Adjustment of the energy level density parameters in this calculation only takes account of accumulation number of the low excited levels compared with the experimental value. The spin cut off factor σ^2 which represents the relation between energy level distribution and angular momentum is not adjusted.

(b) Though multipolar transition about M1, E2, etc. is taken into consideration for the γ transition branch ratio among the low excited separate levels, yet only the E1 process is considered for the transition among the levels in contineous energy region, which will result in certain errors.

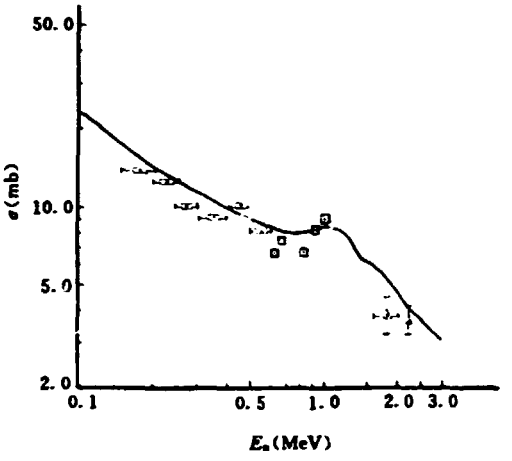

Fig.1 The calculated results of radiative capture cross section $\sigma_{n\gamma}$ for ^{59}Co and those compared with experiments. The experimental values are taken from Ref. [7]

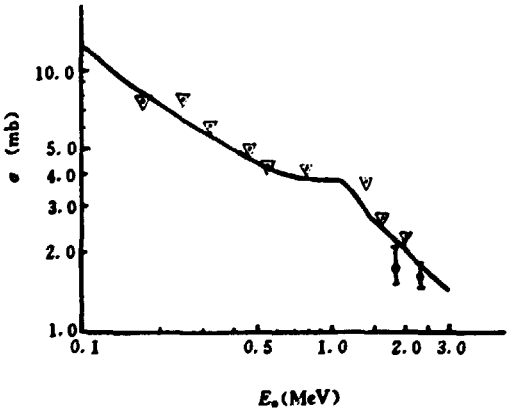

Fig. 2 The calculated results of isomeric state cross $\sigma_{n\gamma m}$ and those compared with experiments. The experimental values are taken from Ref. [7]

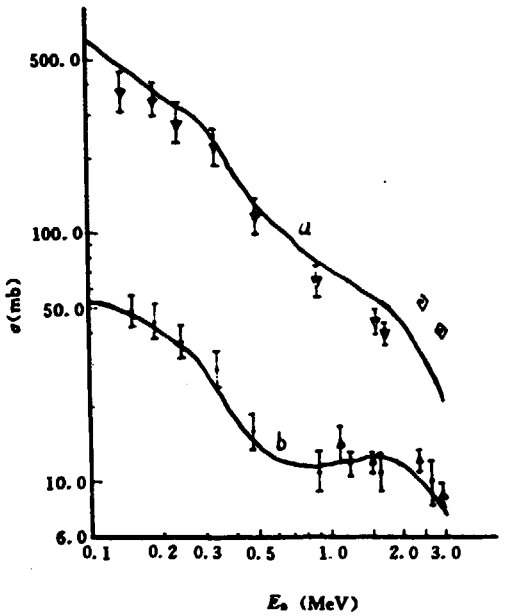

Fig. 3 The calculated results of the ground state cross section $\sigma_{n\gamma g}$ (a) and isomeric state section $\sigma_{n\gamma m}$ (b) for ^{103}Rh and those compared with experiments. The experimental values are taken from Ref. [7]

References

[1] Liu Jianfeng et al., High Energy Physics & Nuclear Physics 5, 469(1990) (in Chinese)

[2] Liu Jianfeng et al., High Energy Physics & Nuclear Physics 4, 349(1991) (in Chinese)

[3] Ma Zhongyu, Chinese Journal of Nuclear Physics 3, 217(1981)

[4] Oblozinsky P. Phys. Rev. C., 2, 407(1987)

[5] Kopesky J. Phys. Rev. C., 5, 1941(1990)

[6] Liu Jianfeng et al., Chinese Journal of Nuclear Physics, 2, 127(1992)

[7] Victoria Mclane et al., Nuclear cross sections, Vol. 2 Neutron cross section curves, National Nuclear Data Center, Brookhaven National Laboratory Upton, New York

[8] Becchetti F. D. et al., Phys. Rev., 182, 1190(1969)

[9] Gilbert A. et al., Can. J. Phys., 43, 1446(1965)

[10] Samuel S. Dietrich et al., Atomic Data and Nuclear Data Tables, 38, 199(1988)

CNP501854

Calculations for n+^{235}U, ^{239,240}Pu Reactions in $E_n = 0.001 \sim 20$ MeV

Yan Shiwei Shen Qingbiao Cai Dunjiu Liang Qichang

(Chinese Nuclear Data Center, IAE)

Cai Conghai

(Dept. of Phys., Nankai University, Tianjin)

Abstract

For the n+^{235}U, ^{239,240}Pu reactions in the energy region of 0.001~20 MeV, the total cross section, the cross section of each opened channels, the elastic / inelastic scattering angular distribution and the secondary neutron energy spectra were calculated by code FUP1. It can be concluded that the calculated results reproduce the experimental data very well.

Introduction

A set of data of fissile nuclei is very important for nuclear reactor designing. However, the obtainable experimental data are rather limited. Thus, it is necessary to use nuclear reaction theory to calculate the related data.

The models used in this calculation include three parts: Optical model [1, 2] (OM), Hauser–Feshbach theory[3] with width fluctuation correction (WHF) and evaporation model[4] including pre–equilibrium (PE) statistical theory based on exciton model. The detail of those theories and the related parameters are shown in the next section.

It should be pointed out that the crucial affairs of this work are to readjusted the related parameters since the obvious discrepancy exists between the results given by the previous parameters[1, 3, 4] and the latest experimental data. Codes ASOP and ASFP[5] were used for searching for the optimal optical potential and fission parameters.

1 Models and Related Parameters

1.1 Optical Model

The spherical nucleus optical model is used in the code FUP1[6]. The related optical model parameters are adjusted automatically by fitting the experimental data and shown in Table 1.

In the high neutron energy range, the contribution of direct reaction becomes important, it was calculated with Coupled Channel Optical Model (CCOM)[2], the deformed optical potential parameters adjusted with CCOM can be read as

(For ^{235}U)

$V = 45.0 - 0.3E_n + 0.006E_n^2$ $\quad R_{so} = 1.12$

$W_S = 3.9 + 0.4E_n$ $\quad A_R = 0.51$

$W_V = 0.0$ $\quad A_S = A_V = 0.50$

$V_{so} = 6.2$ $\quad A_{so} = 0.52$

$R_S = R_V = 1.267$ $\quad \beta_2 = 0.2$

$R_R = 1.285$

(For ^{239}Pu)

$V = 45.25 - 0.25E_n + 0.02E_n^2$ $\quad R_{so} = 1.12$

$W_S = 2.862 + 0.4E_n$ $\quad A_R = 0.62$

$W_V = 0.0$ $\quad A_S = A_V = 0.58$

$V_{so} = 6.2$ $\quad A_{so} = 0.62$

$R_R = R_S = R_V = 1.26$ $\quad \beta_2 = 0.21$

(For ^{240}Pu)

$V = 45.5 - 0.3E_n + 0.006E_n^2$ $\quad R_{so} = 1.12$

$W_S = 2.9 + 0.4E_n$ $\quad A_R = 0.52$

$W_V = 0.0$ $\quad A_S = A_V = 0.50$

$V_{so} = 6.2$ $\quad A_{so} = 0.52$

$R_R = R_S = R_V = 1.267$ $\quad \beta_2 = 0.2$

The direct reaction components are added to the calculated compound nucleus cross section and angular distribution.

1.2 Hauser–Feshbach Theory with Width Fluctuation Correction

In the incident neutron energy region of 10 keV~3 MeV, the WHF theory is employed to calculate the compound–formation cross section, compound elastic scattering cross sections, inelastic scattering cross sections (of discrete levels and continuum), radiative capture cross section, fission cross sections, Legendre coefficients of compound elastic / inelastic scattering angular distributions (for all of the discrete levels), secondary neutron energy spectra of inelastic scattering for continuous states and excitation functions.

In order to calculate transmission coefficients of neutron, fission and radiative capture channels, the giant dipole resonance model of photo–nuclear reaction, fission channel theory based on equivalent single peak barrier are used.

The appropriate fission barrier parameters (V_f and $\hbar\omega_f$ being the height and curvature parameter of the barrier) and the level density parameters (a, being of compound and residual nucleus, a_f, being of the saddle point state) are necessary for this calculation. On the basis of the experimental data[7] as shown in Figs., they are readjusted in the light of the evaluated experimental values of (n,γ), and (n,f) channels cross section. All of the parameters used in this calculation are as the following:

	^{235}U	^{239}Pu	^{240}Pu
V_f	6.2240	6.445	5.796
K_1	2.1616	2.4030	3.5958
K_2	0.1092	0.4982	0.115
E_{pad}	0.65897	1.127019	0.714886

1.3 The Evaporation Model Including Pre–Equilibrium (PE) Statistical Theory Based on Exciton Model

This model is used to calculate the cross section of (n,γ),(n,n'γ), (n,2n), (n,3n), (n,4n), (n,f), (n,n'f), (n,2nf) (n,3nf), (n,F) channels and the normalized secondary neutron spectra in $E_n = 3 \sim 20$ MeV. In order to fit the experimental data well, the level density of the saddle point state is used with two enhancement fitting parameters K_1 and K_2, which are adjusted automatically and given in Table 2.

The Kalbach's constant K, which represents a magnitude of the residual two-body interaction in the pre-equilibrium statistical theory, was selected as $K = 400\ \mathrm{MeV}^{-3}$ through a comparison of the experimental data with calculation. This value is reasonable and consistent with the calculated results using the imaginary part of both the phenomenological optical potential and the microscopic optical potential with Skyrme interaction[8].

2 Summary

The comparison of the calculated results with experimental data is shown in Figs. 1 ~ 5, respectively. It can be concluded that with the new parameters,the calculated results can reproduce experimental data satisfactorily although there is some discrepancy (Fig. 2) between the calculated results of fission cross section and the experimental data at around 18 MeV up to intermediate energy[9]. In fact, this evidence provide the information about the existence of new reaction mechanism and provide a challenge to develop a new model, such as nuclear deformed fluctuation theory.

The data have been adopted for the evaluation of ^{235}U, $^{239,\ 240}Pu$ for CENDL-2.

Table 1 The optical model parameters

	^{235}U	^{239}Pu	^{240}Pu		^{235}U	^{239}Pu	^{240}Pu
a_R	0.414271	0.543281	0.5799	U_2	0.0	0.0	0.0
a_S	0.627889	0.561914	0.5011	V_0	48.177902	48.615433	49.5
a_V	0.627889	0.561914	0.5011	V_1	−0.986129	−0.325505	−0.4397
a_{SO}	0.414271	0.543281	0.5799	V_2	0.052031	0.018296	0.0156
r_R	1.311403	1.267344	1.2632	V_3	−24.0	−24.0	−24.0
r_S	1.276469	1.368766	1.3475	V_4	0.0	0.0	0.0
r_V	1.276469	1.368766	1.3475	V_{SO}	6.2	6.2	6.2
r_{SO}	1.311403	1.267344	1.2632	W_0	9.092310	5.818749	6.405
r_C	1.25	1.25	1.25	W_1	0.015833	0.179633	0.1529
U_0	0.148266	0.530477	1.48	W_2	−12.0	−12.0	−12.0
U_1	0.038355	0.036239	−0.03247				

Table 2 The fission parameters

(for ^{235}U)

	$A+1$	A	$A-1$	$A-2$	$A-3$
V_f	6.0131	5.8374	6.1780	5.9000	
K_1	1.48557	2.73958	1.9599	2.7400	
K_2	0.07537	0.1757	0.3666	0.1760	
Δ	1.1605	0.7454	1.2930	0.69986	1.2900
a	28.6828	28.8197	28.8500	29.0671	28.8999
$\hbar\omega_f$	0.7581	0.5371	0.7581	0.5371	

(for ^{239}Pu)

	$A+1$	A	$A-1$	$A-2$	$A-3$
V_f	6.1580	5.7100	5.4719	5.7100	
K_1	1.95447	1.3361	1.0782	1.34	
K_2	0.623389	0.543879	0.03468	0.5400	
Δ	1.27765	0.748678	0.953856	0.451355	0.95400
a	28.72505	28.403549	28.95265	28.98671	28.99500
$\hbar\omega_f$	0.7051	0.64156	0.70511	0.64156	

(for ^{240}Pu)

	$A+1$	A	$A-1$	$A-2$	$A-3$
V_f	5.3946	6.185	5.553	5.472	
K_1	1.96	1.95	1.009	1.07	
K_2	0.0806	0.623	0.345	0.0347	
Δ	0.749	1.278	0.749	0.950	0.45
a	28.7369	28.725	28.4	28.98	28.987
$\hbar\omega_\gamma$	0.642	0.795	0.652	0.795	

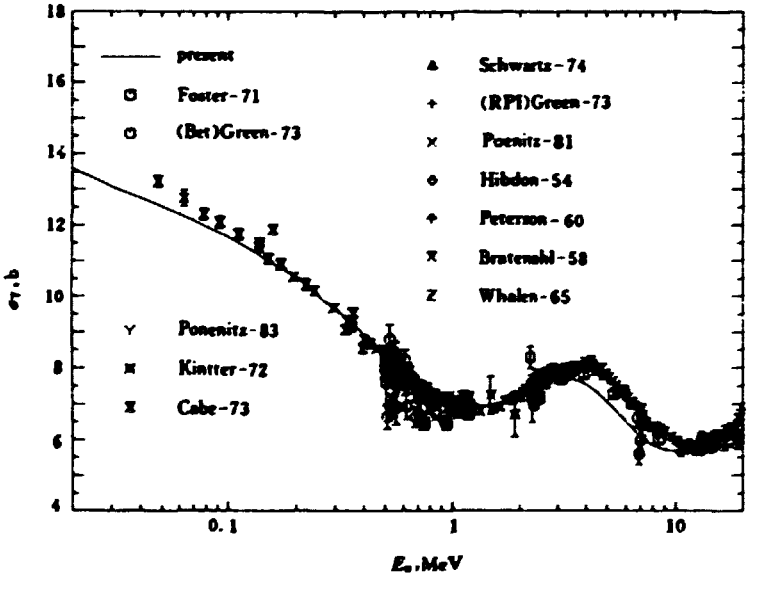

(a)

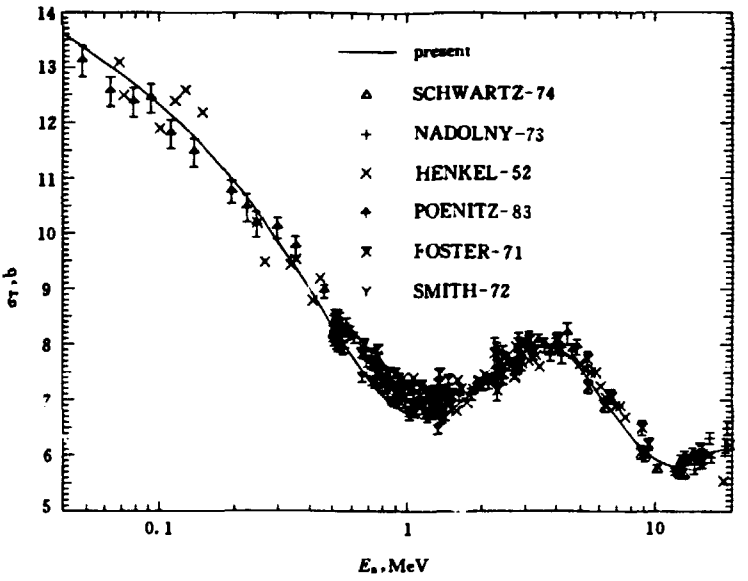

(b)

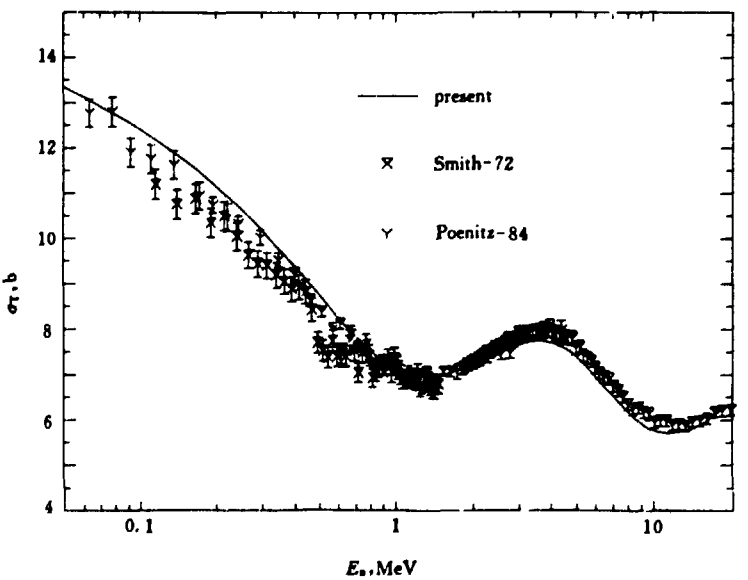

(c)

Fig. 1 The total cross sections for : (a) ^{235}U, (b) ^{239}Pu and (c) ^{240}Pu

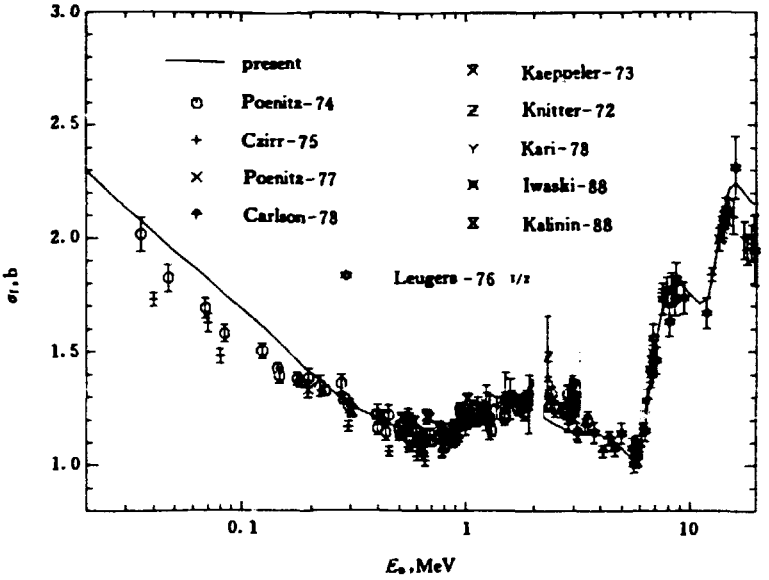
present
Poenitz-74
Czirr-75
Poenitz-77
Carlson-78
Kaeppeler-73
Knitter-72
Kari-78
Iwaski-88
Kalinin-88
Leugers-76
3.0
2.5
2.0
1.5
1.0
0.1
1
10
σ_t,b
E_n,MeV

(a)

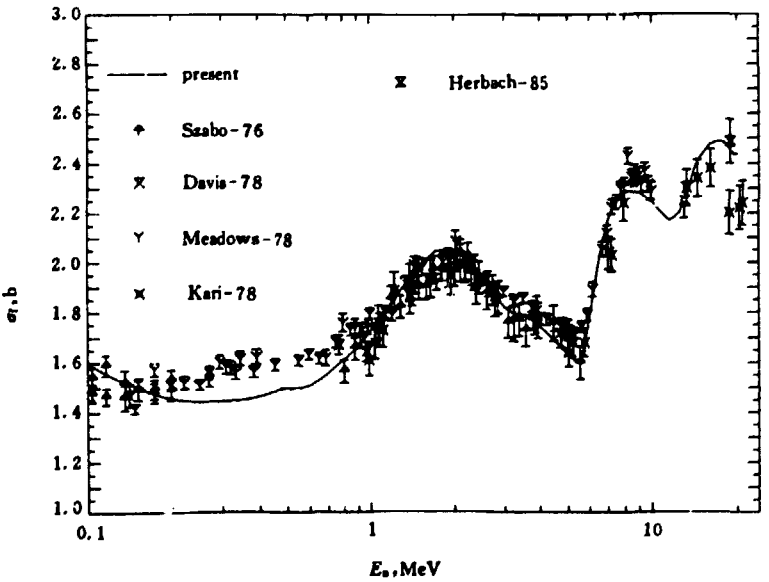
present
Herbach-85
Szabo-76
Davis-78
Meadows-78
Kari-78
3.0
2.8
2.6
2.4
2.2
2.0
1.8
1.6
1.4
1.2
1.0
0.1
1
10
σ_t,b
E_n,MeV

(b)

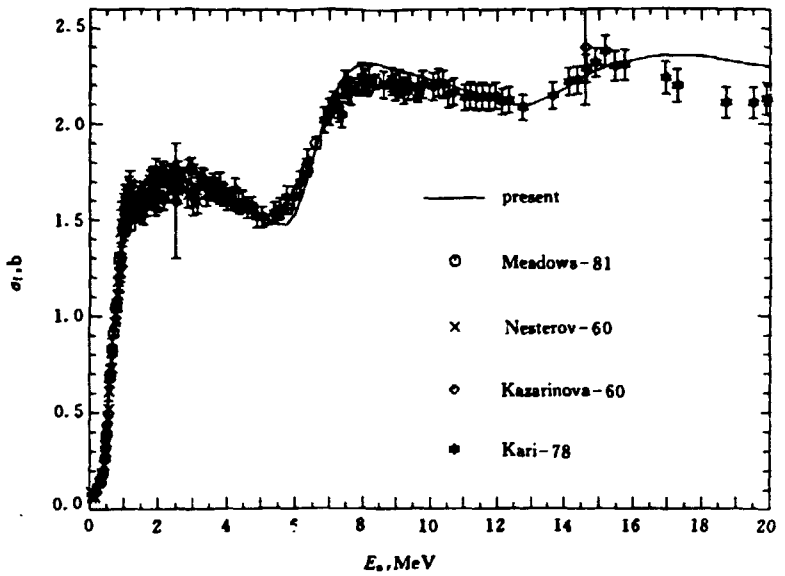

(c)

Fig. 2 The fission cross sections for : (a) ^{235}U, (b) ^{239}Pu and (c) ^{240}Pu

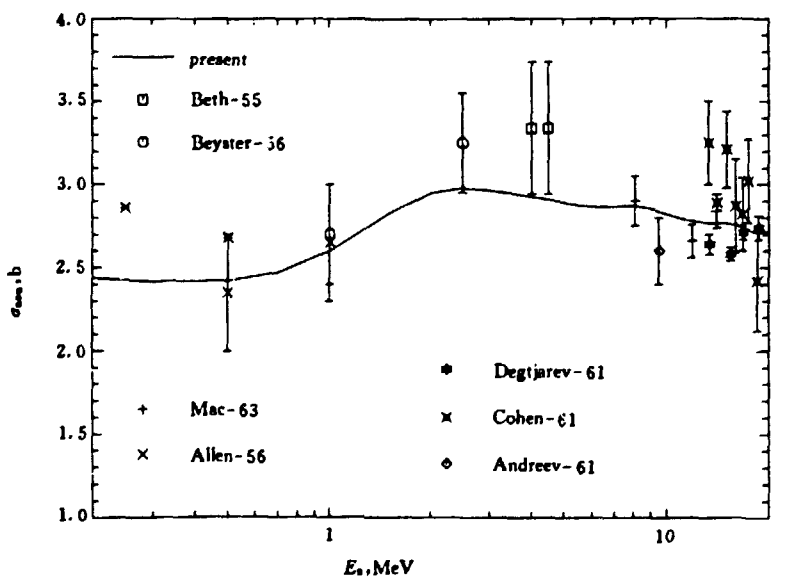

Fig. 3 The non-elastical cross section of ^{235}U

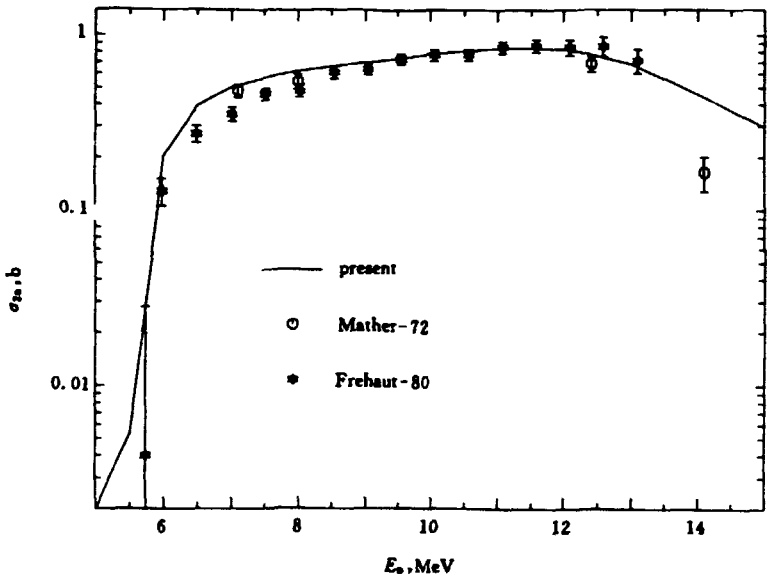

(a)

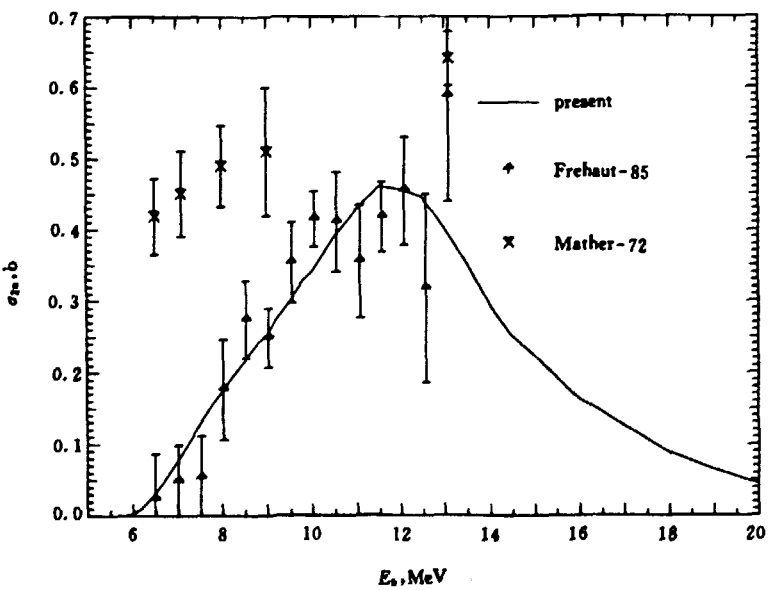

(b)

Fig. 4 The (n,2n) cross sections for : (a) ^{235}U and (b) ^{239}Pu

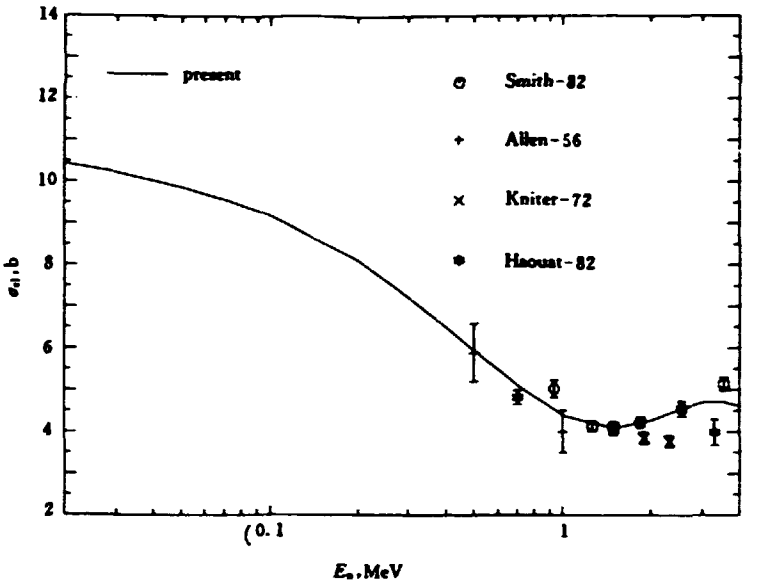

(a)

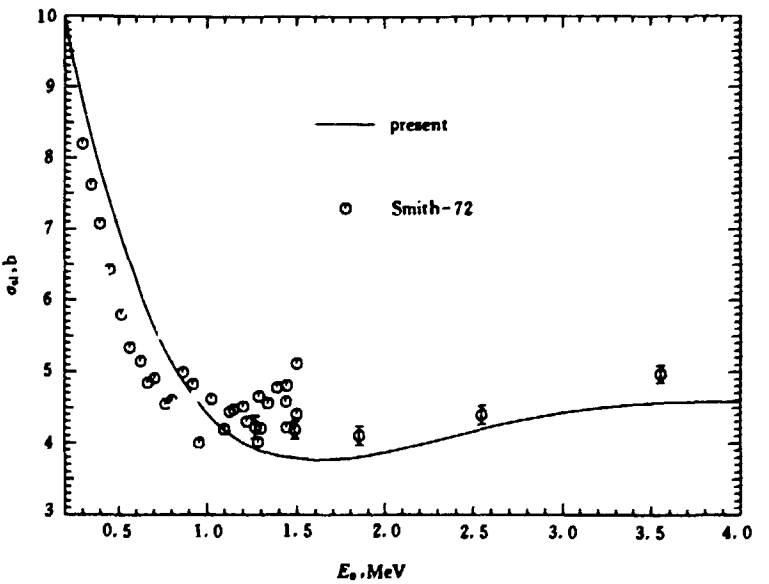

(b)

Fig. 5 The elastical cross sections for : (a) ^{235}U and (b) ^{240}Pu

References

[1] Shen Qingbiao et al., Symposium on Nuclear Reaction Theory and Its Application, published by Atomic Energy Press, Beijing, p. 202, 1980

[2] Zhou Zhining et al., idem, p. 140

[3] Shi Xiangjun et al., idem, p. 260

[4] Zhang Jingshang et al., idem, p. 226

[5] Cai Chonghai, Communication of Nuclear Data Progress, 3, 26(1990)

[6] Cai Chonghai et al., Communication of Nuclear Data Progress, 3, 29(1990)

[7] V. McLANE et al., Neutron Cross Section, published by NNDC / BNL, 1988, New York

[8] Shen Qingbiao et al., Chin. J. Nucl. Phys., Vol. 6, p. 245(1984)

[9] P. W. Lisowski et al., Nucl. Sci. and Eng., 106, 208(1990)

A Comparison of the Maximum Entropy Method of Analysis with the Exciton Model Plus the Master Equation

Yan Shiwei

(Chinese Nuclear Data Center, IAE)

Abstract

The maximum entropy method of analysis is successful in fitting experimental data. In order to reveal the underlying physics, this method is applied in comparison with the conventional approach, i. e the exciton model plus the master equation, to three cases. It is found that both approaches produce almost equally good fits to spectra, and yield almost the same average exciton numbers. This implies that there must be similar physical ideas behind the two approaches, and it should be safe to use the maximum entropy method of analysis to fit data or to estimate reaction cross sections.

Introduction

The maximum entropy method of analysis (hereafter referred to as MEMA. See Ref. [1] and references therein) has been used to analyse heavy ion collision[2~4] and light particle induced reaction[5] and proved to be very successful. But the question still remains to be answered[6, 7]: How much physics can this method tell us ? People may use this analysing method to produce lots of fitting to data but without discovering the physical processes. We feel that the maximum entropy formalism has its profound physical foundation and should agree with other workable theories. It is the purpose of the present paper to make a comparison between the maximum entropy approach and the conventional preequilibrium theory of nuclear reactions induced by light particles. To check carefully its interrelation with other successful theories would surely render some insight into the maximum entropy formalism, and help understand the physical meanings of the Lagrange parameters involved in the maximum entropy distribution. This kind of studies will also provide us with information about the conditions under which the maximum entropy formalism can be used safely to fit data, to investigate the reaction mechanism, or for other purposes.

The entropy of a distribution of outcomes is given by[14]

$$S = -\sum_{f=1}^{N} P_f \ln P_f \tag{1}$$

It is non-negative and reaches its maximal value for a uniform distribution when all outcomes are equal probably. If the states f are grouped together such that there are g_γ states in the group γ and only the probabilities P_γ of the different groups are given, we assign equal probability to all the state f within any particular group. The probability of any one quantum state within the group γ is thus given by

$$P_f = \frac{P_\gamma}{g_\gamma} \tag{2}$$

and hence

$$S = -\sum_{f=1}^{N} \frac{P_\gamma}{g_\gamma} \ln \frac{P_\gamma}{g_\gamma} = -\sum_{\gamma} P_\gamma \ln \frac{P_\gamma}{g_\gamma} \tag{3}$$

The prior distribution is defined as the one of maximum entropy

$$P_\gamma^{(0)} = \frac{g_\gamma}{\sum_\gamma g_\gamma} = \frac{g_\gamma}{N} \tag{4}$$

So that

$$S = \ln N - \sum_\gamma P_\gamma \ln \frac{P_\gamma}{P_\gamma^{(0)}} \tag{5}$$

Here $\ln N$ is the maximum value of the entropy. The entropy S has been identified as the information provided when the distribution P_γ has been determined.

The basic idea[1~4] of the maximum entropy approach is that if without any interreaction happening, the system is described by a statistical distribution, where all final quantum states (on the energy shell) are equally probable, but in a real reaction the system is described by a distribution which is subjected to constraints imposed by the dynamics of the collision and which should be as statistical as possible. The maximum entropy distribution for the final states is

$$P_\gamma^{\mathrm{ME}} = P_\gamma^{(0)} \exp\left[-\lambda_0 - \sum_{i=1}^{n} \lambda_i A_i(\gamma) \right] \tag{6}$$

where λ's are the Lagrange multiplies. This distribution involves n constraints,

$$\langle A_i \rangle = \sum_\gamma A_i(\gamma) \qquad i = 1, \cdots, n$$

where $A_i(\gamma)$ is the value of the constraint for the group of final states γ. In practice, only two constraints are rather well established and found to be important, i. e. the average value of the excitation energy E^* and the average value of its square root $E^{*1/2}$. So, the maximum entropy fitting formula which is now widely used is

$$P^{\mathrm{ME}}(E^*) = E_f^{\frac{1}{2}} E^{*-\frac{5}{4}} \exp\left[2\sqrt{aE^*} - \lambda_0 - \lambda_1 E^* - \lambda_2 E^{*\frac{1}{2}} \right] \tag{7}$$

where $a \approx A/8$ is the level density parameter, and E_f is the kinetic energy of the final channel which is related to the excitation energy E^* according to the following expression:

$$E_f = E_i + Q_{gg} - E^* \tag{8}$$

where E_i is the incident energy and Q_{gg} is the ground state to group state Q value. λ_2 is related to the average exciton number according to

$$\langle n \rangle = \frac{2\sqrt{3\langle E^* \rangle}}{\pi}\left(a^{\frac{1}{2}} - \frac{\lambda_2}{2} \right) \tag{9}$$

where $\langle E^* \rangle$ is the average excitation energy. We point out here that Eq. (9), although widely used, is obtained only from the level density consideration. In the present work, we compare the MEMA formula, Eq. (9), with the conventional preequilibrium theory, i. e. the exciton model plus the master equation (hereafter referred to as EMPME), which has been very successful in describing both heavy-ion and light-particle induced reaction.

In section 1, we give a brief description on the formulas of MEMA and EMPME. Section 2 contains the results of the two theories and a brief discussion. The conclusion is drawn in section 3.

1 Formalism

For the maximum entropy calculation, we use Eq. (7) to fit experimental spectra. The parameter λ_0 only serves as a normalization constant. The parameters λ_1 and λ_2 are determined by the following two nonlinear equations:

$$\int E^* f(E^*)\, dE^* = \int E^* P^{ME}(E^*)\, dE^* \tag{10}$$

$$\int E^{*\frac{1}{2}} f(E^*)\, dE^* = \int E^{*\frac{1}{2}} P^{ME}(E^*)\, dE^* \tag{11}$$

where $f(E^*)$ is the experimental spectrum to be fitted with Eq. (7). Suppose that both $f(E^*)$ and $P^{ME}(E^*)$ are normalized. To facilitate solution of Eqs. (10) and (11), we can start with an estimate of the two unknown parameters λ_1 and λ_2, given by the experimental spectrum $f(E^*)$ which is roughly

parameterized with E_m^*, the value of E^* at which $f(E^*)$ reaches its maximum, and Γ, the full width, as shown in Fig. 1. We use the following expressions for the estimated λ_1 and λ_2 :

$$\lambda_2 \approx 2a^{\frac{1}{2}} - 4E_m^{*\frac{3}{2}}\left[\frac{8\ \ln 2}{\Gamma^2} - \frac{1^*}{2(E_i + Q_{gg} - E_m^*)} + \frac{5}{4E_m^*}\right] \tag{12}$$

$$\lambda_1 \approx \frac{a^{\frac{1}{2}} - \frac{\lambda_2}{2}}{E_m^*} - \frac{1}{2(E_i + Q_{gg} - E_m^*)} - \frac{5}{4E_m^*} \tag{13}$$

which are straightforward.

For the conventional EMPME calculation of preequilibrium reactions, we use our code to calculate angle-integrated cross sections. For the formalism, see Refs. [7] and [8]. Let $Q(n,\vec{\Omega},t)$ denote the occupation probability for the composite nucleus state $(n,\vec{\Omega})$ at time t, where n is the exciton number and $\vec{\Omega}$ is the direction of the fast particle. The generalized master equation then reads:

$$\begin{aligned}\frac{\mathrm{d}}{\mathrm{d}t}Q(n,\vec{\Omega},t) = &\sum_m \int Q(m,\vec{\Omega}',t)W_{m\to n}(\vec{\Omega}',\vec{\Omega})\ \mathrm{d}\vec{\Omega}' \\ &- \sum_m \int Q(m,\vec{\Omega}',t)W_{n\to m}(\vec{\Omega},\vec{\Omega}')\ \mathrm{d}\vec{\Omega}'\end{aligned} \tag{14}$$

where

$$W_{m\to n}(\vec{\Omega}',\vec{\Omega}) = \lambda_{m\to n}G(\vec{\Omega},\vec{\Omega}') \tag{15}$$

The transition rate $\lambda_{m\to n}$ from the state m to the state n can be expressed as follows:

$$\begin{aligned}\lambda_{n\to n+2} &= \frac{2\pi}{h}KA^{-3}E^{*\,n-1}\frac{g(gE^*)^2}{2(n+1)} \\ \lambda_{n\to n-2} &= \frac{2\pi}{h}KA^{-3}E^{*\,n-1}\frac{gph(n-2)}{2} \\ \lambda_{n\to n} &= \frac{2\pi}{h}KA^{-3}E^{*\,n-1}\frac{g(gE^*)}{2n}[p(p-1)+h(h-1)+4ph]\end{aligned} \tag{16}$$

where E^* is the excitation energy of the composite system, A is the mass number of composite system, p and h are the particle and hole number, respectively, and g is the single particle level density. The parameter K corre-

sponds to the strength of interactions which lead to transition between exciton states, and is adjusted in accordance to the systematic by Kalbach et al.[9, 10] to get the best fit to experimental spectra. We will not list all the formulas used here because they can be found in many articles, e. g. Ref. [8]. We only need the time– and angle–integrated occupation probabilities

$$P_n = \int Q(n,\vec{\Omega},t)\ \mathrm{d}\vec{\Omega}\ \mathrm{d}t \tag{17}$$

Then, the angle–integrated cross section for the emitted particle i is expressed as:

$$\frac{\mathrm{d}\sigma^i(\varepsilon)}{\mathrm{d}\varepsilon} = \sum_n \frac{\mathrm{d}\sigma^i_n(\varepsilon)}{\mathrm{d}\varepsilon}$$

$$\frac{\mathrm{d}\sigma^i_n(\varepsilon)}{\mathrm{d}\varepsilon} = P_n W^i_n(\varepsilon) \tag{18}$$

where i represents the proton or neutron. The emission probability $W^i_n(\varepsilon)$ for the particle i from the exciton state n is given as

$$W^i_n(\varepsilon) = \frac{2S_i + 1}{\pi^2 h^3}\mu_i \frac{p(n-1)}{gE^{*(n-1)}}\varepsilon\sigma_i(\varepsilon)(E^* - B_i - \varepsilon)^{n-2} \tag{19}$$

where S_i and μ_i are the spin and the reduced mass for the particle i, B_i is its binding energy in the composite system, and $\sigma_i(\varepsilon)$ is the inverse cross section for forming the compound system by the particle i with kinetic energy ε.

We define the average exciton number $\bar{n}$ according to the occupation probabilities of exciton states :

$$\bar{n} = \frac{\sum_n nP_n}{\sum_n P_n} \tag{20}$$

The two average exciton numbers, $\bar{n}$, calculated by using EMPME and $\langle n \rangle$, calculated by using MEMA, will be compared, and the comparison will reveal some very important features of the maximum entropy approach.

2 Results And Discussion

We have applied both MEMA and EMPME to three cases: $^{209}Bi(p,p')$ at 62 MeV, CsI(n,p) at 21.5 MeV, and CsI(n,p) at 18 MeV.

In Figs. 2~4, we have plotted the experimental spectra[11, 12] (crosses), and the corresponding fits produced by using MEMA (solid line) and EMPME (dashed line) for the three cases, respectively.

The parameters used in the calculation are given in Table 1. In MEMA, the parameters λ_1 and λ_2 are adjusted to get the best fit to the experimental spectra, while in EMPME, the parameter K is adjusted in accordance to the systematics of Kalbach et al.[9, 10] to get the best fit to data. We see that the calculated spectra are in general in rather good agreement with the experimental data. Also given are the central results of the present work, i. e. values of $\langle n \rangle$, the average exciton number in MEMA, and $\bar{n}$, the average exciton number in EMPME. We see that in general MEMA and EMPME yield very close values of the average exciton numbers.

It is not difficult to understand why MEMA and EMPME give almost the same exciton numbers. It is simply due to the fact that both MEMA and EMPME involve the following physical ideas: The system develops as statistically as possible, i. e. the final states are occupied with the probabilities which are controlled mainly by the corresponding total available phase space[13] but subjected to the same correction. We will have a more detailed discussion in another paper on the interrelation between the underlying physical ideas of MEMA and EMPME.

3 Conclusion

In conclusion, we emphasize that MEMA can furnish good fits to the spectra of light particle induced reactions, and yield average exciton numbers which agree quite well with those given by EMPME. Our study here shows that it is safe to use MEMA to produce fits to data, at least in the domain in which EMPME can be used successfully. Because MEMA is sophisticated and easy to manipulate, MEMA could be a very powerful tool in practice, especially in projecting our knowledge of cross sections from the energies for which there are experimental data available to the energies for which there are no data available. This could be of great interest especially to the people who are engaged in nuclear data calculation and evaluation.

Table 1 Parameters used in the numerical calculation and the calculated average exciton number $<n>$ (for MEMA) and $\bar{n}$ (for EMPME)

	^{209}Bi(p,p′) (62 MeV)	CsI(n,p) (21.5 MeV)	CsI(n,p) (18 MeV)
λ_1 (MeV)$^{-1}$	0.0926	0.90995	1.0977
λ_2 (MeV)$^{-1/2}$	8.3695	0.8580	0.2292
$<E^*>$ (MeV)	21.48	22.30	18.6
K	150	50	45
$<n>$	8.0	17.8	17.6
$\bar{n}$	5.4	17.1	19.2

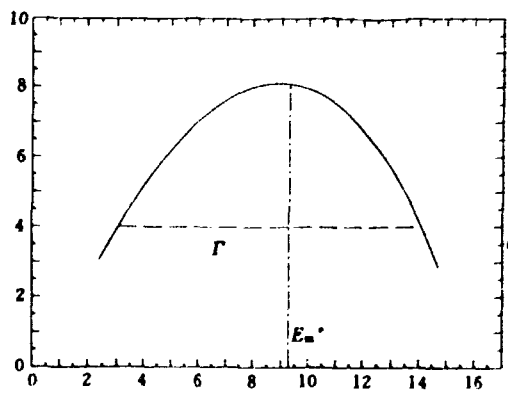

Fig. 1 Schematic plot of the experimental spectrum $f(E^*)$ roughly parameterized with E^* at which $f(E^*)$ reaches its maximum and the full width

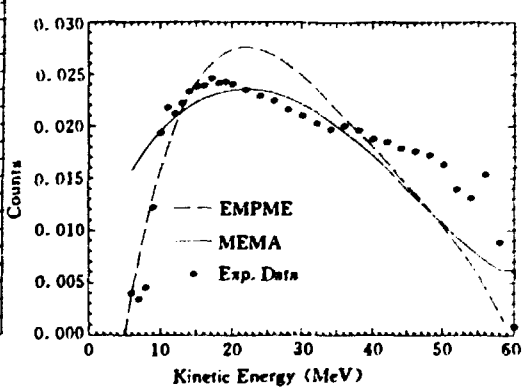

Fig. 2 The cross section for reaction ^{209}Bi(p,p′) at 62 MeV

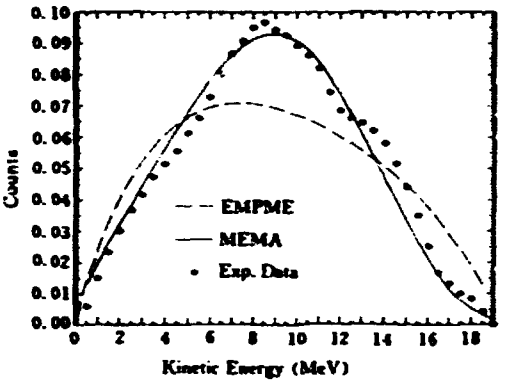

Fig. 3 Same as in Fig. 2 but for the reaction CsI(n,p) at the beam energy 21.5 MeV

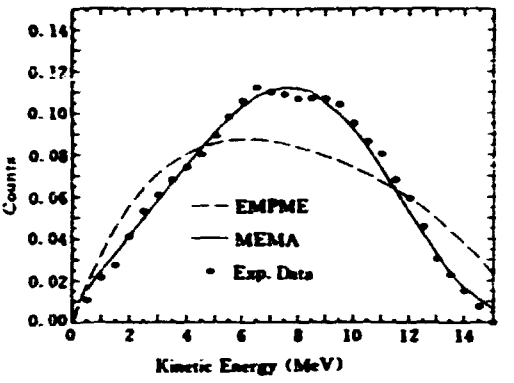

Fig. 4 Same as in Fig. 2 but for the reaction CsI(n,p) at the beam energy 18 MeV

References

[1] E. T. Jaynes, in "The Maximum Entropy Formalism", MIT Press, 1978

[2] Y. Alhassid, R. D. Levine, Phys. Rev. A18, 89(1978)

[3] Y. Alhassid, R. D. Levine, J. S. Karp, S. G. Steadman, Phys. Rev. C20, 1789(1979)

[4] J. S. Karp, S. G. Steadman, S. B. Gazes, R. Ledoux, F. Videback, Phys. Rev. C25, 1838(1982)

[5] T. Tsukamoto, Y. Kawazoe, preprint, 1982

[6] S. Marsh, Phys. Lett. 121B, 238(1982)

[7] Z. Y. Sun, S. N. Wang, J. S. Zhang, Y. Z. Zhuo, Z. Phys., A305, 61(1982)

[8] A. Iwamoto, K. Harada, Proc. Int. Symp. on Light Ion Reaction Mechanism, Osaka(1983)

[9] C. Kalbach-Cline, Nucl. Phys. A210, 590(1973)

[10] C. Kalbach, Z. Phys., A287, 319(1978)

[11] F. E. Bertrand, R. W. Peelle, Phys. Rev. C8, 1045(1973)

[12] L. Milazzo-Colli et al., Phys. Lett. 36B, 447(1971)

[13] H. A. Weidenmuller, Progress in Particle And Nuclear Physics, Vol. 3, p. 49~126, 1980

[14] S. Goldman, "Information theory", Dover, New York, p. 47, 1953

CNPSO1856

A Processing Code System AUTOOPT Searching for Optimal Neutron Optical Potential Parameters

Liu Tong Zhao Zhixiang

(Chinese Nuclear Data Center, IAE)

Abstract

A processing code system searching for optimal neutron optical potential parameters is introduced, and a general box diagram as well as typical results for ^{51}V are given.

Introduction

Theoretical calculation plays an important role in the neutron data evaluation. Searching for the optimal neutron optical potential parameters is the first step for a consistent theoretical calculation. Although a lot of computer codes can be used to search for optimal neutron optical potential parameters, automatically, the input format is very complex, especially for input of the experimental data. This affair will cost the evaluator a lot of time to input the experimental data in the format which fit the code. For filling the input data and plotting output data automatically or half–automatically, a code system — AUTOOPT is developed. This code also has a function to plot the results to compare with the experimental data .

1 The Functions of AUTOOPT Code System

This code system has the following functions :

1.1 Filling the input data for the code, automatically

1.2 Plotting the result compared with the experimental one

2 The Source of Input Parameters and Experimental Data

Mass of target is obtained from a table of mass for about 108 nuclei; The

initial values of optical potential parameters are obtained from the systematics[1]; Giant resonance parameters and the parameters for discrete levels are obtained from CENPL[2] —"Chinese Evaluated Nuclear Parameter Library"; Experimental data are obtained from the EXFOR retrieving system [3]; Other parameters are fixed in the code, the user can easily change these parameters by changing a default data file.

3 The Codes Searching for Optimal Optical Potential Parameters

There are several codes searching for optical potential parameters. Up to now, only two codes, APOM94 — a new version of code APOM [4], and GENOA[5] are included in this code system.

4 The Design of AUTOOPT

The code system includes a lot of computer codes, and the EXFOR retrieving system as well as the CENPL library. Therefore, it is impossible to use one code to carry out these functions. Several small codes are used and the VMS commands are also used to connect all the codes together. For this reason, the code system can not be used on the other computer easily.

General box diagram of AUTOOPT is shown in Figs. 1~2. The meaning of some major blocks in the box diagram is as follows:

START — Input the charge number and mass number of target. The mass number equals zero means a natural element.

DLS-END — Obtaining the parameters for every discrete level from CENPL.

SETUP — Set up the environment for EXFOR retrieving system.

CRE-CSRET1, CSRET, PRE-CSTTOL1, CSTTOL — Retrieving the total cross section of EXFOR data and changing the format.

CRE-CSRET2, PRE-CSTTOL2 — Same as CRE-CSRET1 and PRE-CSTTOL1, for the nonelastic cross section.

PRE-DISTTOL, CRE-DISRET, DISRET — Retrieving the elastic angular distribution, and change to CM system.

CHEXP, CHECK, INT-ELCS, CHANG — For interpolation and check the EXFOR data to fit the code (APOM94 or GENOA).

BIND-END — Obtaining the mass of target.

PRE-APOMI4, PRE-APOMI5 — Preparing the input data APOM94I4.DAT and APOM94I5.DAT for APOM94 code.

PRE-PRE-GENOA, PRE-GENOA — Preparing the input data

FOR050.DAT for code GENOA.

APOM94, GENOA–N — Two codes searching for optimal optical potential parameters.

PLT–APOM, PLT–GENOA — Plotting the results for APOM94 and GENOA, respectively.

OPT–APOM, OPT–GENOA — Changing the optimal neutron optical potential parameters to the standard format, the format can be easily used as input data of the DWUCK[6] code and the UNF[7] code.

5 The merit of this code system

5.1 Although the code system is complex, but the user does not need to know details about the codes, the user can simply use the following command to start the system,

```
$ @DUB0:[L.OPT]AUTOOPT
```

5.2 Deleting the intermediate–file or files automatically.

5.3 Sometimes the coordinate system of elastic angular distribution need to be changed from LAB to CM system, but in the EXFOR data, some flag which is used to express the coordinate system of angle are missing . So, a small code is used to decide the coordinate system of angle according to whether the data are exactly equal degree or not.

6 A Typical Example

The code system AUTOOPT has been used to search for the optimal neutron optical potential parameters for ^{51}V by using the APOM94 code. Fig. 3 shows a typical result for total cross section. Because many experimental data are available for the total cross section, this code system divides the whole energy region (0 ~ 20 MeV) into 20 energy interval, and the interpolation values at each energy interval are plotted in Fig. 3. The typical results for elastic angular distribution are shown in Figs. 4~5. From these figures, it can be seen that present results are consistent with the measured data of I. H. Towle[8] for Fig. 4 and R. D. Lawson[9] for Fig. 5.

Acknowledgement

The authors would like to give their thanks to "the Science Foundation for

Young Scientist of CIAE" for its support to this work, and Dr. Shen Qingbiao, the author of code APOM94, for his helpful advice.

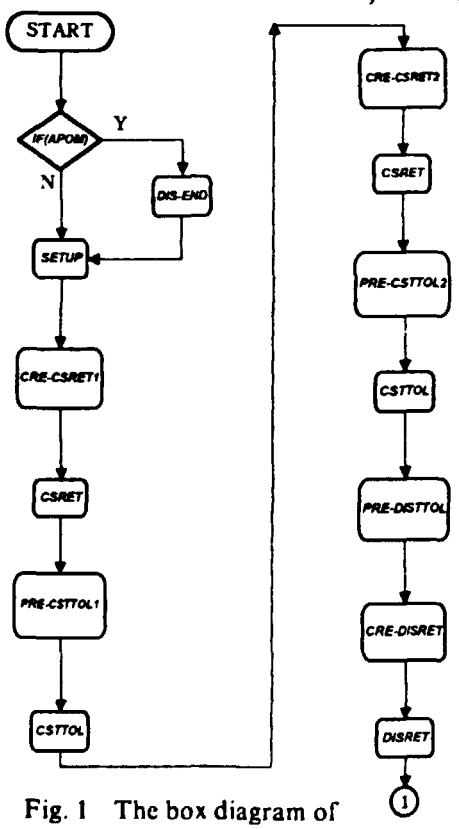

Fig. 1 The box diagram of AUTOOPT (part 1)

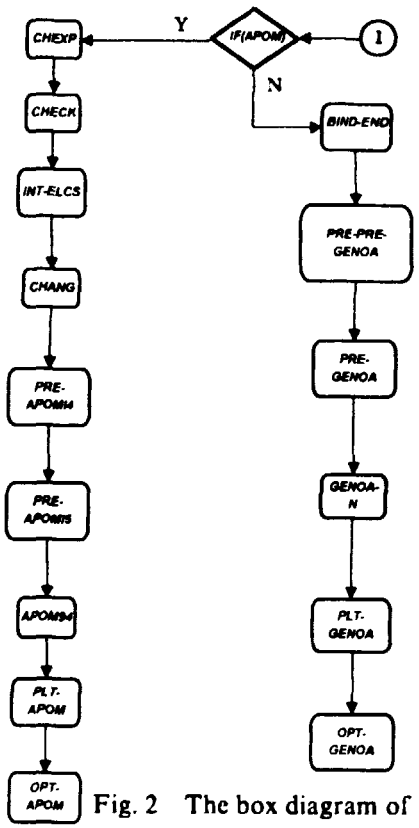

Fig. 2 The box diagram of AUTOOPT (part 2)

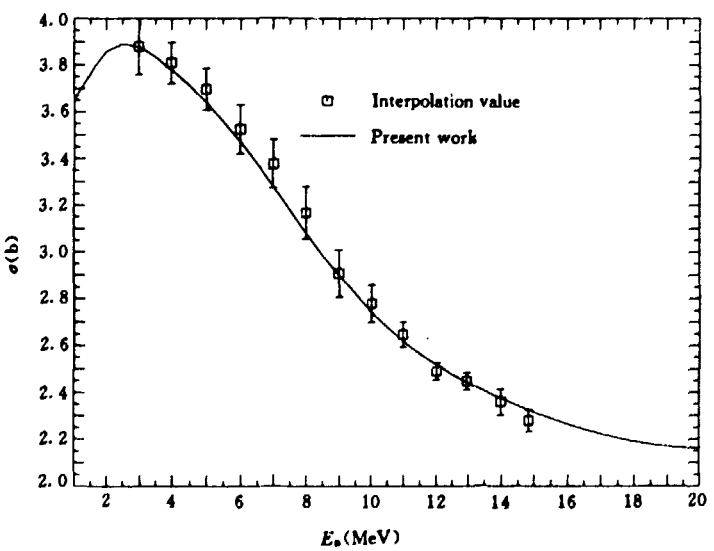

Fig. 3 Comparison of total cross sections with experimental data for ^{51}V

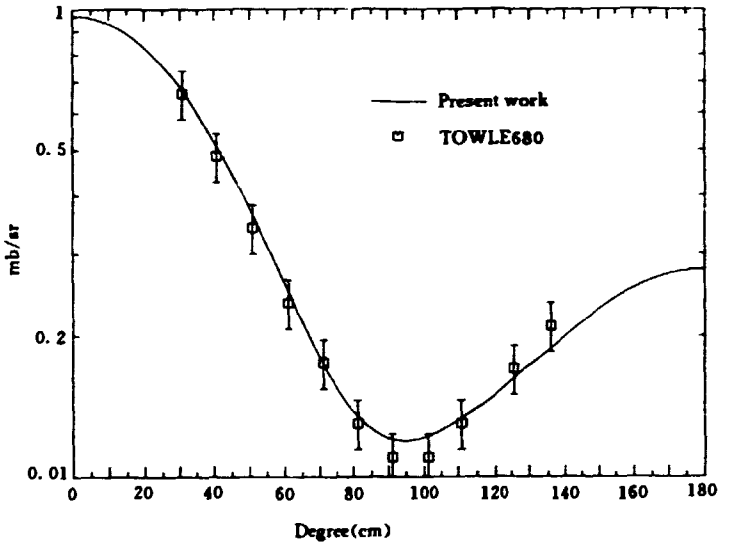

Fig. 4 Comparison of elastic angular distribution with experimental data at incident energy 1.61 MeV for ^{51}V (CM System)

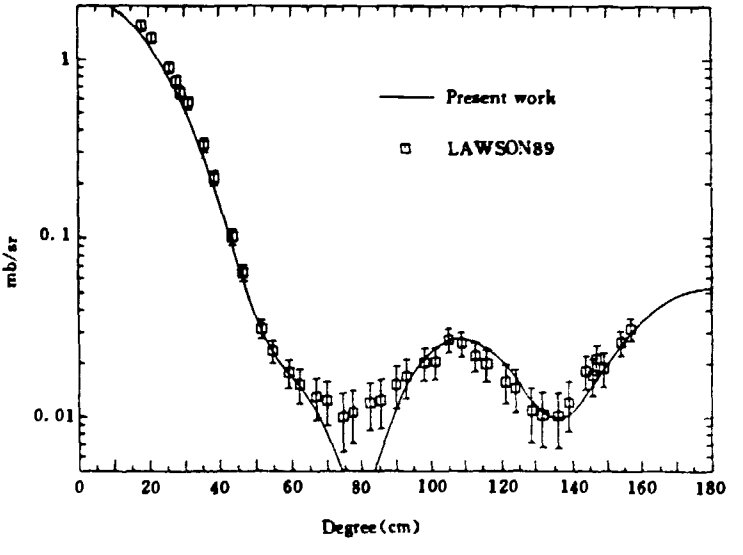

Fig. 5 Comparison of elastic angular distribution with experimental data at incident energy 9.5 MeV for ^{51}V (CM System)

References

[1] Perey C. M. et al., Atomic Data and Nuclear Data Tables, Vol. 17, No. 1, p. 1(1976)
[2] Su Zongdi et al., CNDP, No. 7, p. 73(1992)
[3] Liang Qichang et al., CNDP, No. 9, p. 72(1993)
[4] Shen Qingbiao, CNDP, N0. 7, p. 43(1992)
[5] Perey, F. G. and Zhao Zhixiang, Private communication (1990)
[6] Kunz, P. D. and Zhao Zhixiang, Private communication (1990)
[7] Zhang Jingshang, CNDP, No. 7 p. 14(1992)
[8] Towle J. H., J, NP / A, 117, 657(1968)
[9] Lawson R. D. et al., J, NP / A, 493, 267(1989)

The Pre– and Post–Management of Code DWUCK4

Yan Shiwei

(Chinese Nuclear Data Center, IAE)

P. D. Kung's DWUCK program is a main code to calculate direct reaction data with distorted–wave Born approximation and widely used in studying nuclear reaction mechanism and analysing experimental information, especially, calculating nuclear data. Unfortunately, the preparation of the input data is an arduous affair for multi–point of incident particle energy and multi–level calculation; secondly, the angular distribution of direct reaction is given as $\sigma(\theta)$ for each angle θ, not the coefficient f_l of Legendre expansion, which is necessary for other related code (i. e. UNF) and ENDF / B library format.

In this work, code DPPM, an auxiliary program for pre– and post–management of the input and output parameters of code DWUCK4, is presented for the convenient use of code DWUCK4.

The main improvement is for the following points :

1. The input file DPPMI.DAT can be written with the free format. The DPPM can automatically produced INTER.DAT which is used to check the input data in terms of DWUCK4's requirement.

2. Multi-energy points and multi-level circulation.

3. Coupling of angular momentum

For a+A→B*+b reaction, the conservation of angular momentum and parity should be guaranteed, which can be expressed as:

$$\vec{J}_A + \vec{S}_a + \vec{L}_{aA} = \vec{J}_B + \vec{J}_b + \vec{L}_{bB}$$
$$\pi_a \pi_A \pi(-)^{L_{aA}} = \pi_b \pi_B (-)^{L_{bB}}$$

where $\vec{J}_A$, $\vec{S}_a$ are the angular momentum of target and incident particle, $\vec{L}_{aA}$ is the relatively orbital angular momentum of incident channel, $\vec{J}_B$, $\vec{J}_b$, $\vec{L}_{bB}$ are the corresponding quantum of final channel. π_i is the parity of each particle.

The orbital angular momentum transfermation is

$$\vec{J} = \vec{J}_B - \vec{J}_A$$
$$\vec{S} = \vec{S}_b - \vec{S}_a$$
$$\vec{L} = \vec{J} - \vec{S}$$

L obey the parity conservation with

$$\pi_a \ \pi_A \ \pi_b \ \pi_B = (-1)^L$$

For a specific reaction a+A→B*+b, DPPM code can automatically couple the angular momentum $\vec{J}_A$, $\vec{S}_a$, $\vec{J}_B$, $\vec{J}_b$ with π_a, π_A, π_b, π_B

4. Legendre expansion of angular distribution

The angular distribution of direct reaction is given as $\sigma(0)$ for each angle 0 with DWUCK program, which have to be changed into Legendre expansion as:

$$\sigma(0) = \frac{\sigma}{4\pi} \sum_{l=0}^{\infty} (2l+1) f_l P_l(\cos 0)$$

with

$$\int_{-1}^{1} P_k(x)P_l(x)\,dx = \begin{cases} 0 & k \neq l \\ \dfrac{2}{2l+1} & k = l \end{cases}$$

so

$$f_l = \frac{2\pi}{\sigma}\int_0^{\pi} \sigma(\theta)P_l(\cos\theta)\sin\theta\,d\theta$$

Angular distribution is given out as the Legendre coefficients in file FL.DAT

CNPSO1858

III DATA EVALUATION

A Code for Supplement of Gamma Production Data to Evaluated Neutron Data

Zhao Zhixiang Liu Tong

(Chinese Nuclear Data Center, IAE)

Abstract

A code for supplement of gamma production data to evaluated neutron data is developed on the basis of semi-empirical formulae. The major functions of the code are described. A box diagram and a computational example are given.

Introduction

Gamma production data such as gamma spectra and multiplicity are very important in coupled neutronics-photonics calculation for nuclear energy applications. Unfortunately, most of evaluations in CENDL-2 did not include such data. Recently, a semi-empirical method to supplement gamma production data has been developed on the basis of evaporation model and exciton model[1]. Compared to the consistent theory model calculation, the semi-empirical method does not depend on the detailed knowledge of nuclear properties and allows to do separative calculation without re-evaluating the cross sections, angular distributions and spectra of the secondary neutron. Based on the semi-empirical formulae presented in Ref. [1], a code, MAIN-GAM is developed to help evaluator supplement gamma production data to evaluated neutron data file. The code is capable of calculating the total gamma spectra at given incident neutron energy to compare with measured one and of generating a new evaluated data file with gamma production data satisfying energy balance from the "old evaluated data file".

1 The Functions of MAIN-GAM

(1) Adjusting Parameters to Fit Measured Data

The MAIN–GAM can calculate the gamma spectra and multiplicity at given incident neutron energy. The product of normalized spectra and multiplicity for given reaction is multiplied by cross sections taken from " old evaluation data". The total gamma spectrum is obtained by summing up the spectra over all reactions. The user can fit the experimental data by adjusting two parameters R and E_R, where E_R is the giant dipole resonance energy and R is a constant in the systematics of nuclear temperature in the level density formula :

$$T = R / \sqrt{A}$$

where A is the mass number of the nucleus. In the case of no measured gamma spectra are available, $R = 23$ is used, and E_R is calculated by the following formula :

$$E_R = 16.8 - 0.02A$$

(2) Supplement of Gamma Production Data

For the evaluated data which did not include the gamma production data, the MAIN–GAM can supplement gamma production data in rather convenient manner for evaluator and does not need to re–evaluating the cross sections, angular distributions and spectra of secondary neutrons.

Firstly, the user must adjust parameters by using the function 1 if measured data are available, and then through re–running the code, a new set of evaluated data including gamma production data is generated.

In order to make new data file be consistent with old evaluation data, the following rules are taken into account by MAIN–GAM code :

a. Only the reaction channel which appear in file 3 can be given in files 12, 14, and 15.

b. The data for non–threshold reaction should cover the energy range from 10^{-5} eV to 20 MeV and those for threshold reaction should be given from threshold energy up to 20 MeV.

c. In order to keep the energy balance for the Q value which is used in gamma production data calculation must be consistent with those in the old evaluated file.

(3) The Correction for Energy Balance

Because the performance of MAIN–GAM is not a consistent calculation

with what the evaluator did in the old evaluation, sometimes, the total output energy is larger than the energy available more or less. Therefore, the correction of energy balance is needed for these reactions.

The MAIN–GAM carry out the energy correction through revising multiplicity M_γ, calculated by MAIN–GAM as M'_γ:

$$M'_\gamma(\mathrm{i}) = M_\gamma(\mathrm{i}) \times \alpha_\mathrm{i}$$

$$\alpha_\mathrm{i} = 1 - \frac{E_{\mathrm{tot}}(\mathrm{i}) - E_{\mathrm{ava}}(\mathrm{i})}{E_\gamma(\mathrm{i})} - \frac{1}{A}$$

where $E_{\mathrm{tot}}(\mathrm{i})$ and $E_\gamma(\mathrm{i})$ are average energy for neutron+gamma+recoil and for gamma calculated by MAIN–GAM for reaction i, respectively; E_{ava} is the available energy .

2 General Design of MAIN–GAM

General box diagram of MAIN–GAM is shown in Fig. 1 and the detailed description for "Multi–energy points loop" and for "Fill ENDF / B data" are shown in Fig. 2 and Fig. 3. In the next, the meaning of some major blocks in the box diagram are explained in detail.

GAMMA — To calculate gamma production spectra and multiplicity at given incident energy. Eight reactions, including (n,γ), (n,n'), (n, 2n), (n,3n), (n,p), (n,pn+np), (n,α) and (n,nα+αn), are taken into account.

PREGAM can calculate the input data for subroutine GAMMA. Among these input data, the separation energies of the outgoing particle from the residuals for the reaction process are calculated by using a table of mass automatically, and the cross sections for the reactions are read from file 3 of "old evaluation data".

This subroutine has two choices, one is for single energy point calculation, another is for multi–energy points.

SEPIN — To prepare input data for GAMMA subroutine.

SEPOUT and CHUNIT — These two subroutines can store the data (the output result of GAMMA) according to the MF number, and then, change the unit to be consistent with the ENDF / B format.

CREATE ENERGY POINTS — Total 21 energy points are generated for the subroutine GAMMA. The first one is 10^{-5} eV, and then from 1 MeV to 20 MeV, the energy interval is 1 MeV.

SEARMT and SUBNB — To read information from file 3, and decide which reaction should be supplemented or not, as well as select the first energy point of the reaction to be supplemented.

ADDMF1, ADDMF12, ADDMF14 and ADDMF15 — To supplement the MF = 1 (MT = 451), 12, 14, and 15, respectively. The user can easily change the information in MF = 1, MT = 451 by re-writing the file 1451.LIS. An isotropic distribution for all photons is assumed for MF = 14.

COPREST — To copy the rest part of "old evaluation data" to the "new evaluation data".

READ12, GETALPHA, MUTIA, REWRITE — To do the correction for energy balance.

3 The Application of the Code MAIN-GAM

For Ti, Zn, Zr, Mo, Cd, In, Sn, Sb, Hf, Ta, W, ^{197}Au and Pb, the supplement of gamma production data for CENDL-2 has been carried out by using the MAIN-GAM code[2].

MAIN-GAM is developed on MICRO-VAX-II and the SUN working station, the source code is available from the authors.

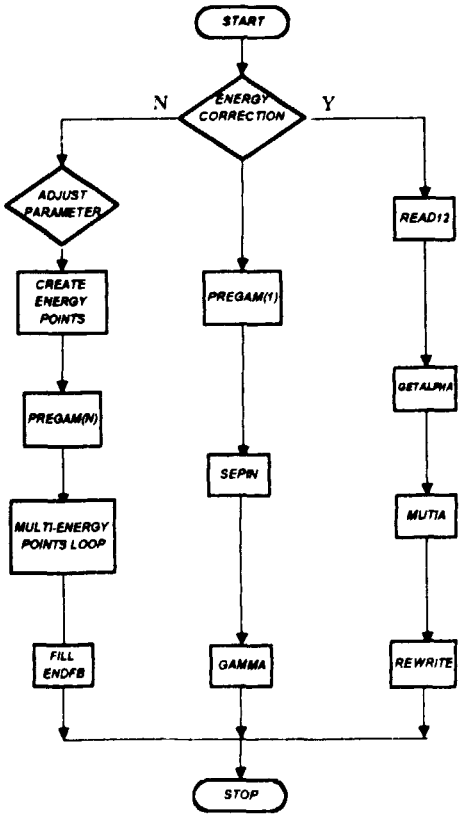

Fig. 1 Box diagram of MAIN-GAM

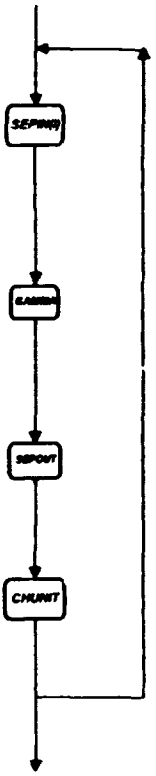

Fig. 2 Box diagram for "Multi-Energy Points Loop"

Fig. 3 Box diagram for "Fill ENDFB"

Acknowledgment

The authors would like to give their thanks to Dr. Han Yinlu for using his code for binding energy calculations.

References

[1] Zhao Zhixiang, Liu Tong, "Semi-empirical Method of Calculation of Continuum Gamma Spectra and Multiplicity", to be published

[2] Zhao Zhixiang, Liu Tong, "Calculation of Gamma Production Data from Neutron Induced Reactions on Thirteen Targets", to be published

CNPSO 1ASP

The Update and Modification of the Total Cross Sections of CENDL-2 for CENDL-2.1

Liu Tingjin Sun Zhengjun

(Chinese Nuclear Data Center, IAE)

Through the intercomparisons of Fe, Cr, Ni data among CENDL-2, JENDL-3, ENDF / B-6 and BROND-2, some problems have been found for the total cross sections in CENDL-2, mainly the losses of the resonance structures for some medium-weight nuclide due to sparse energy points[1]. To make clear that for how many and which nuclides the problems exist, the total cross sections of 18 nuclides (P, S, K, Fe, Cr, Ni, Ti, V, Zr, Nb, Cd, In, Sn, Sb, Hf, Ta, W, Pb) from CENDL-2, were intercompared. As a result, there are the problems for the data of 7 nuclides, and they were updated and improved. The following is a brief introduction.

1 S

The total cross sections in the energy region 3.5~8 MeV were modified. The experimental data (S. Cierjacks, GERKFK, 6806) were used. In the energy region 3.5~4.5 MeV, they were recommended directly, from 4.5 to 8 MeV, they were averaged over each 3 energy points by using code SEL[2], except the peaks at about 5.0 and 5.4 MeV, which were also recommended directly. Using CRECTJ5[3], the data file was made, and the energy meshes and their cross section consistency were adjusted by doing $\sigma_{n,n} = \sigma_t - \sigma_{non}$ and $\sigma_t = \sigma_{n,n} + \sigma_{non}$.

The part of improved cross sections, as an example, is given in Fig. 1.

2 K

The total cross sections in the energy region 0.36~7 MeV were modified. The experimental data (S. Cierjacks, GERKFK, 1969) were used. In the energy region 0.36~5 MeV, the energy points were selected, taking one of each two, keeping the peaks and valleys, and in the energy region from 5 to 7 MeV, the data were averaged over each 3 energy points. The experimental data processing was completed with code SEL[2]. The cross section consistency and energy

meshes of the cross section were adjusted by using CRECTJ5[3] in the same way as S nuclide.

The part of improved cross sections, as an example, is given in Fig. 2.

3 Ti

The total cross sections in the energy region 0.1～20 MeV were modified. The data were replaced by the corresponding data taking from JENDL-3[4]. The processing and consistency adjustment were completed by using CRECTJ5[3] in the same way as nuclide S.

The part of improved cross sections, as an example, is given in Fig. 3.

4 Zr

The total cross sections in the energy region 0.84～0.93 MeV were modified. There are unreasonable structures in this energy region, it was smoothed by eye guide. The nonelastic cross section was checked, there is no such unreasonable structures. The cross section consistency and their energy meshes were adjusted by using CRECTJ5[3] in the same way as S nuclide.

The modified cross section is given in Fig. 4.

5 Sb

The total cross sections in the energy region 2.5～5 MeV were modified. The data were replaced by the corresponding data taking from JENDL-3[4]. The processing and consistency adjustment were completed by using CRECTJ5 in the same way as S nuclide.

The part of improved cross sections, as an example, is given in Fig. 5.

6 Hf

The total cross sections in the energy region 15～20 MeV were improved. The new experimental data (W. P. Poenitz, USAANL, 8305) were fitted with spline program[5]. The fit data were used to replace old ones.The processing and cross section consistency were adjusted by using CRECTJ5 in the same way as sulphur nuclide.

The modified cross sections are given in Fig. 6.

7 Pb

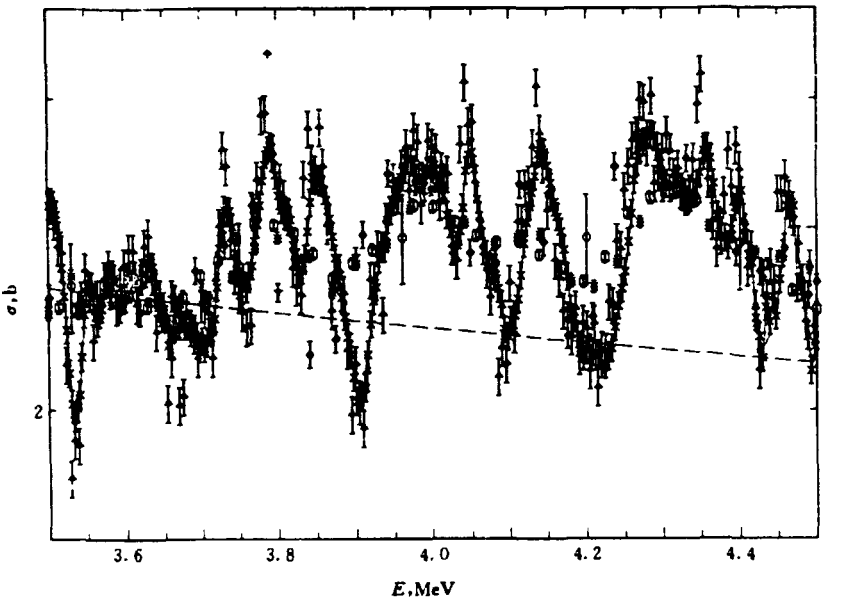

Fig. 1 The modified total cross sections for ^{16}S

— CENDL-2.1; —· ENDF / B-6; -- JENDL-3; □ D. G. Foster JR, 1usabnw (7102);

△ A. D. Carlson, 1usawis (67); × S. Cierjacks, 2gerkfk (6806);

† J. Cabe, 2FR BRC (7311); ⋇ R. Ricamo. 2swteth (5103).

⊙ N.NERESON,1USALAS(5302) ▼ G.H.STAFFORD,2UK CAV(51)

✚ M.K.MACHWE,1USABAR(59) ✳ P.CUZZOCREA,2ITYCAT(6011)

◇ K.TSUKADA,2JPNJAE(6305)

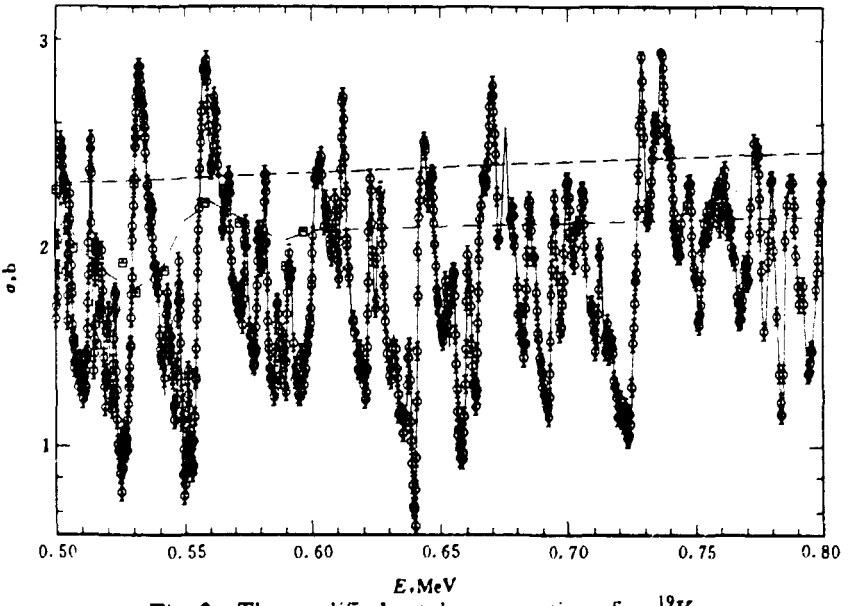

Fig. 2 The modified total cross sections for ^{19}K

—— CENDL-2.1; —·— ENDF / B-6; --- JENDL-3.

□ R. E. Peterson, iusawis (5003); ⊙ S. Cierjacks, 2gerkfk (6902).

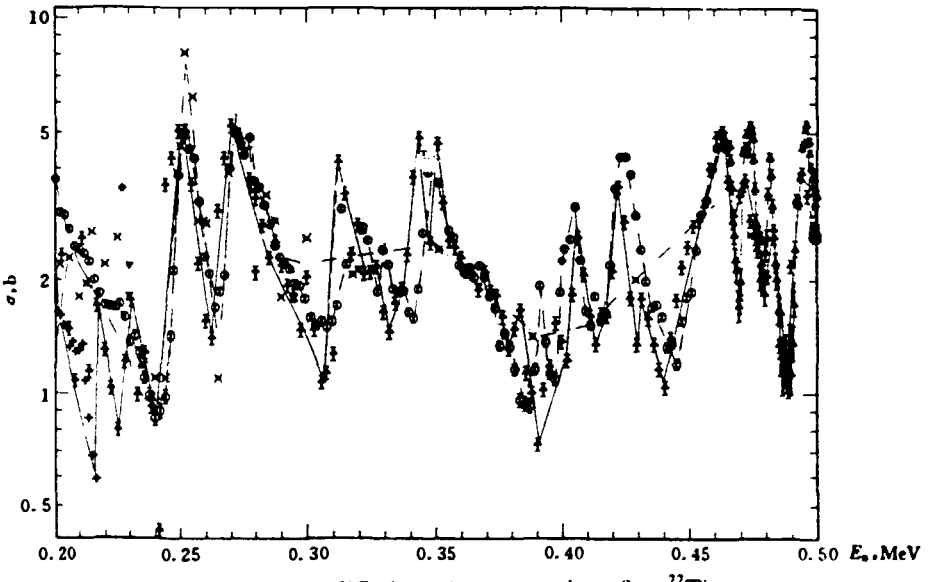

Fig. 3 The modified total cross sections for ^{22}Ti

— CENDL-2.1; —· ENDF/B-6; -- JENDL-3; —· · CENDL-2.

□ R.B.SCHWARTZ,1USANBS(7401)
△ E.BARNARD,1USAANL(7409)
× H.W.NEWSON,1USADKE(61)
◆ J.CABE,2FR BRC(7311)
⊙ E.BARNARD,1USAANL(7409)
+ J.B.GARG,1USACOL(7106)
◇ R.K.ADAIR,1USAWIS(5003)
▼ V.V.FILIPPOV,4CCPFEI(68)

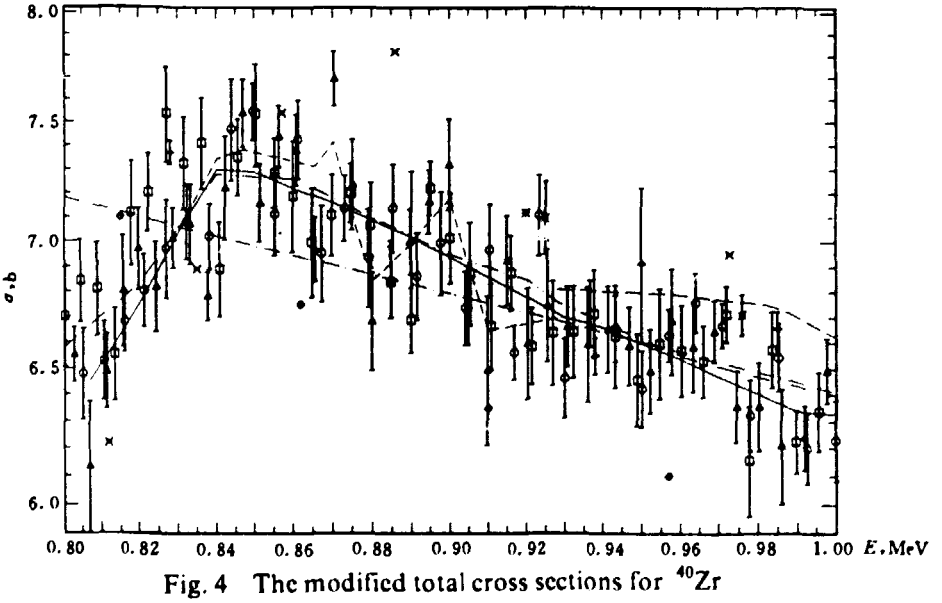

Fig. 4 The modified total cross sections for ^{40}Zr

— CENDL-2.1; -·- JENDL-3; -- CENDL-2; —— BROND-2; —· · ENDF/B-6.

□ L.GREEN,1USABET(7304)
△ L.GREEN,1USABET(7304)
× C.K.BOCKELMAN,1USAWIS(4907)
◆ W.P.POENITZ,1USAANL(8305)
⊙ L.GREEN,1USABET(7304)
+ R.W.STOOKSBERRY,1USABET(7306)
◇ J.B.GUERNSEY,1USAMIT(5601)
▼ W.P.POENITZ,1USAANL(8305)

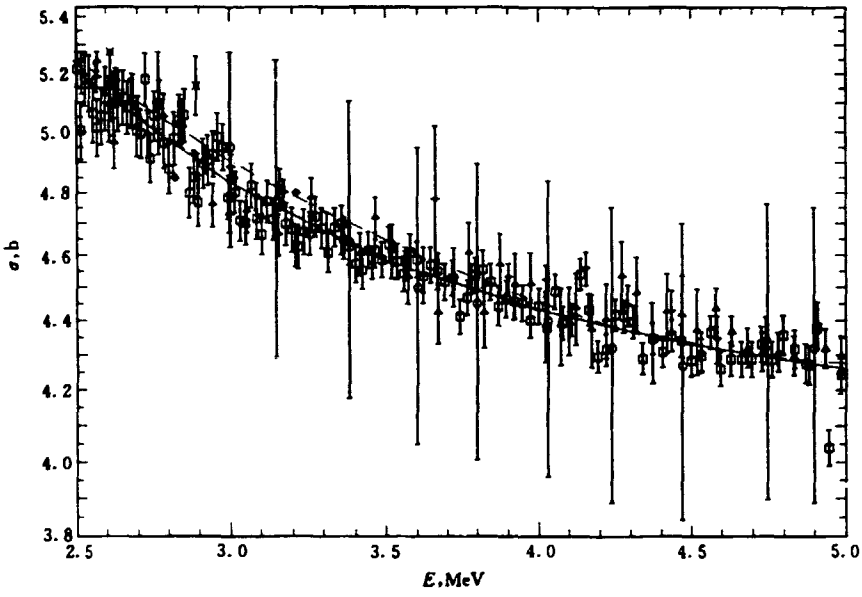

Fig. 5 The modified total cross sections for ^{51}Sb

— CENDL-2.1; —· CENDL-2; --- JENDL-3.

□ D.G.FOSTER JR,1USABNW(7102)
△ A.D.CARLSON,1USAWIS(67)
× L.D.VINCENT,1USATNC(60)
✦ A.B.SMITH,1USAANL(8403)
✱ K.KOBAYASHI,2JPNKTO(8908)
⊙ N.NERESON,1USALAS(5406)
✚ D.W.KENT,1USABAR(62)
◇ D.W.MILLER,1USAWIS(5210)
▽ W.P.POENITZ,1USAANL(8305)
✳ K.KOBAYASHI,2JPNKTO(8908)

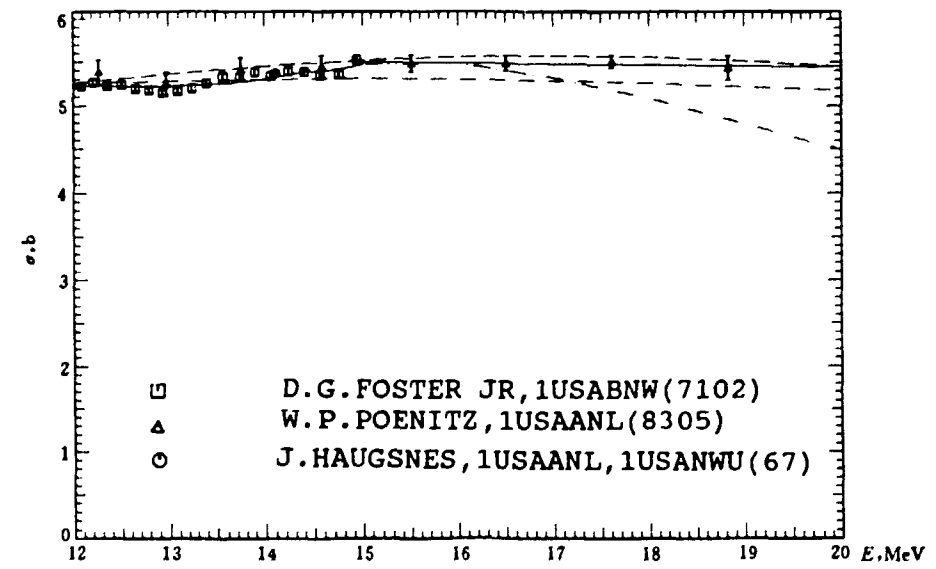

Fig. 6 The modified total cross sections for ^{72}Hf

— CENDL-2.1; -·- ENDF/B-6; -- JENDL-3; -··- CENDL-2.

The total cross sections in the energy region 0.47~5 MeV were modified. The experimental (R. B. Schwartz, USANBS, 7401) and JENDL-3 data were used in the energy region 0.47~3 and 3~5 MeV respectively. For experimental data, the energy points were selected, taking one of each two, keeping the peaks and valleys, using code SEL. The data file making and cross section consistency adjustment were completed by using program CRECTJ5 in the same way as S nuclide.

The part of improved cross section, as an example, is given in Fig. 7.

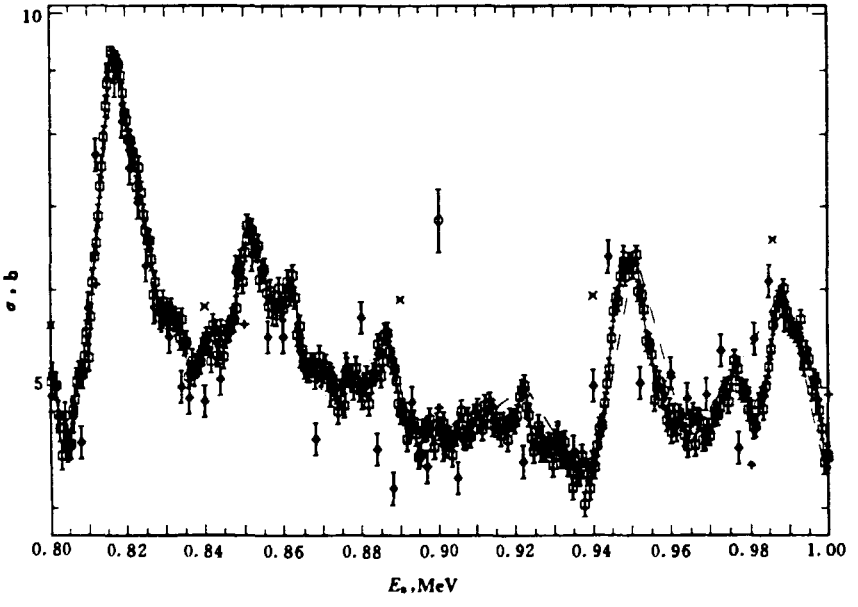

Fig. 7 The modified total cross sections for ^{82}Pb

— CENDL-2.1; -·- JENDL-3; —— BROND-2; -··- CENDL-2.

□ R.B.SCHWARTZ,1USANBS(7401)
△ R.FIELDS,1USAANL(4704)
× H.B.WILLARD,1USAMIT(5009)
✦ W.B.GILBOY,2UK ALD(6303)
⊙ W.E.GOOD,1USAUI (4105)
+ C.K.BOCKELMAN,1USAWIS(4907)
◇ J.CABE,2FR BRC(6706)

References

[1] Liu Tingjin et al., Proc. of International Conference on Nuclear Data for Sci. & Tech., A28, Gatlinburg, USA (1994)

[2] Liu Tingjin, Internal report (1989)

[3] T. Nakagawa, private communication (1989)

[4] H. D. Lemmel, IAEA-NDS-110 (1992)

[5] Liu Tingjin et al., CNDP, 2, 58(1989)

CN9501860

Evaluation of Neutron Monitor Cross Section for $^{197}Au(n,2n)^{196}Au$ Reaction from Threshold to 80 MeV

Yu Baosheng Shen Qingbiao Cai Dunjiu

(Chinese Nuclear Data Center, IAE)

Introduction

The evaluation of intermediate energy nuclear data for the $^{197}Au(n,2n)^{196}Au$ reaction cross section is very important to monitor high energy neutron field, neutron activation, dosimetry and radiation induced material damage etc..

This work was undertaken to provide more precise and complete intermediate energy monitor reaction data of $^{197}Au(n,2n)^{196}Au$ from threshold to 80 MeV. The measured data for $^{197}Au(n,2n)^{196}Au$ cross section up to 29 MeV were collected and analysed. In order to predict the data in higher energy region the theoretical calculation of above mentioned reaction was carried out. Then a set of cross sections for $^{197}Au(n,2n)^{196}Au$ reaction was recommended on the basis of experimental and calculated data.

1 Analysis and Treatment for Experimental Data

The available measured data[1~22] of $^{197}Au(n,2n)^{196}Au$ reaction exist below 29 MeV, seen in Table 1, Fig. 1 and, Fig. 2. Most of the experimental data up to 1994 have been included. Many data were retrieved from EXFOR master files of International Atomic Energy Agency, new information on experimental results from CIAE and Southwest Institute of Nuclear Physics and Chemistry in China was added.

Among 22 references there are 21 ones provided the data around 14 MeV. For evaluating the cross section at 14.7 MeV, all collected data were adjusted for energy and cross section to equivalent 14.7 MeV, depended on the shape of the excitation curve for $^{197}Au(n,2n)^{196}Au$ reaction. In order to obtain the factors of energy adjustment values, the data of Ryves et al.[14] were used. The data around 14 MeV were also renormalized, using the same standard cross section given in Ref. [22].

The relevant cross sections and energy adjusted factors R_1 and R_2 are also given in Table 1. separately, in which σ_0 and σ represent the original and adjusted cross sections, respectively.

The abundance of isotope ^{197}Au in natural gold is 100% . The half-life of ^{196}Au is very well known with the value of 6.18 days, the characteristic gamma ray of 356 keV of the product has a branching ratio of 87.6% . The characters of gamma ray of ^{196}Au have not change to any significant extent for many years. The errors due to uncertainties in decay data were small and were within the quoted errors. Therefore, the half-life and branch ratio for this reaction were unnecessary to do any revision

After adjustment, the first-phase evaluation was done for twenty-one cross section values at 14.7 MeV. Some data should be rejected due to the large discrepancies with others and exceeding the averaged value by three standard deviations.

The second step was made by the averaging with the weighted factor for the adjusted data. The weighted factors in the evaluation were based on the given errors by the authors and quoted errors by us. Present evaluated data are 2133± 34 mb at 14.7 MeV, as shown in Fig. 3. The data measured by Bayhurst[9] , Veeser[11] , Csikai[15] , Ikeda[18] , Greendwood[19] , Wang Xiuyuan[21] and Zhao Wenrong[22] are in good agreement with the obtained recommended value by us at 14.7 MeV.

The data obtained by Bayhurst[9] supersede all their earlier results provided by Prestwood[3] and extend to the extent of 30 MeV using (t,n) neutron source. Veeser[11] adopted the direct detection technique for emitted neutrons by using a large liquid scintillator. The data measured by Veeser[11] were similar to the tend obtained by Bayhurst[9] up to 24 MeV energy region. The measured data from Garlea[17], Frehaut[13], Paulsen[10] and Bayhurst[9] provided the tend of excitation function for $^{197}Au(n,2n)^{196}Au$ reaction below 12 MeV. For the energy region, Paulsen[10] adopted the measurement method relative to a standard cross section in order to avoid the effect of no correction for the distinction of coming neutron energy in sample. The data finished by Frehaust are similar to the results by Bayhurst[9].

These experimental data mentioned above are quite adequate to a complete shape of excitation function for $^{197}Au(n,2n)^{196}Au$ reaction from threshold to 30 MeV. The evaluated result was obtained from these data by using a program of orthogonal polynomial fitting.

2 Supplement the Scarce Data in High Energy Range

To supplement the scarce data for $^{197}Au(n,2n)^{196}Au$ reaction in high energy range, the theoretical data calculated by SPEC[23] were adopted. The model parameters including a set of optimum optical potential parameters, level density parameters as well as exciton model constant were carefully selected. The calculated data can reproduce the total, nonelastic cross section and elastic scattering angular distributions very well from 0.5 to 80 MeV. The various calculated data such as (n,γ), (n,p), (n,α), etc. are in agreement with the experimental data.

According to the model parameters used, the predicated neutron reaction $^{197}Au(n,2n)^{196}Au$ cross sections was calculated from threshold to 80 MeV.

The theoretical calculated values were very closed to the experimental data, which almost overlap with the experimental data between 28 and 30 MeV. Therefore, the calculated data above 30 MeV were recommended, as shown in Fig. 1.

Acknowledgements

The authors are indebted to IAEA (International Atomic Energy Agency), CNNC (China National Nuclear Corporation) and CIAE for their supports, and thank to Drs. N. P. Kocherov, T. Benson, O. Schwerer, Lu Hanlin and Zhao Wenrong for their kind help and suggestions.

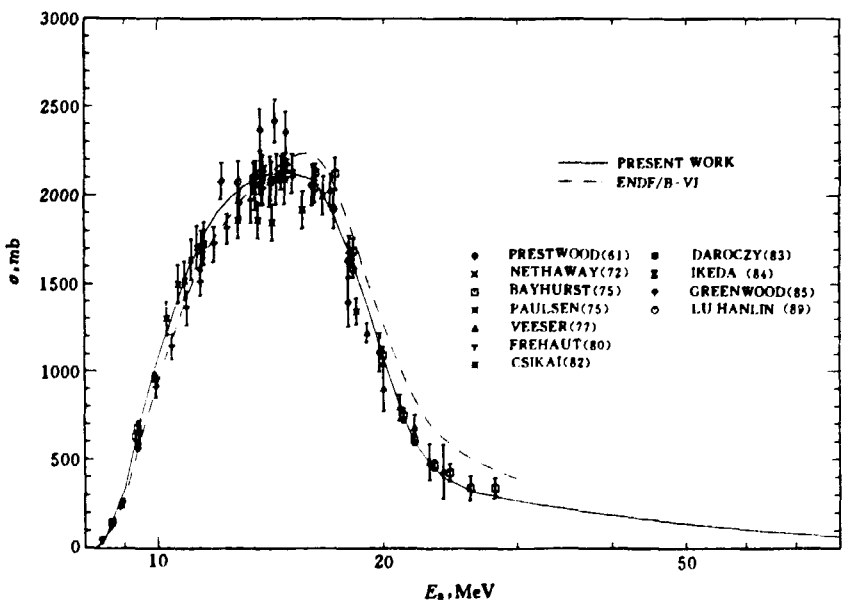

Fig. 1 Comparison among evaluated data with measured data for Au(n,2n) reaction cross section

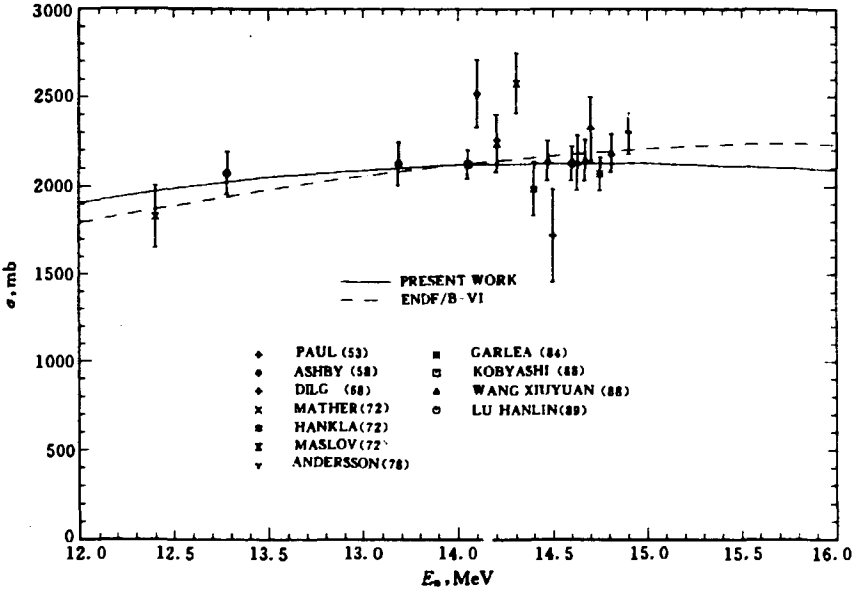

Fig. 2 Comparison among evaluated data with measured data for Au(n,2n) reaction cross section

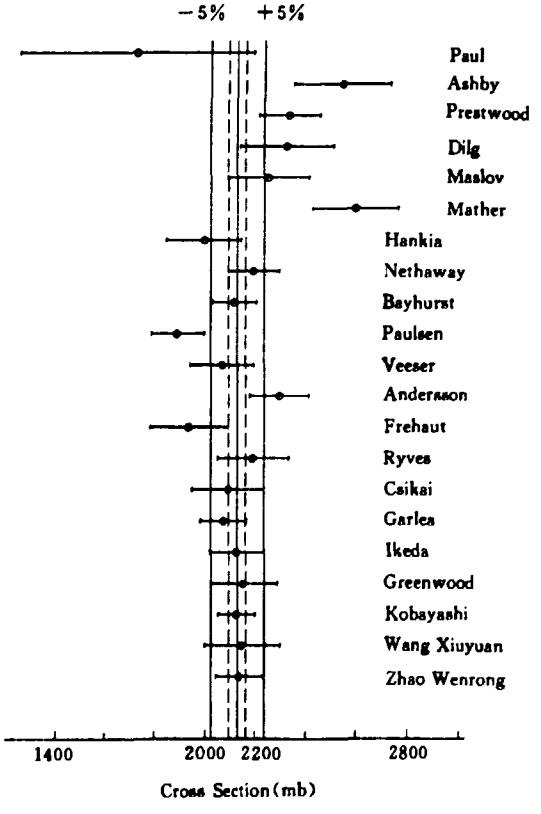

Fig. 3 Evaluation of 14.7 MeV data for Au(n,2n) reaction

Table 1 Collected data and relevant information for $^{197}Au(n,2n)$

No.	Year	Author	E_n MeV	σ_0, mb	$\Delta\sigma$ mb	n flux	R_1	R_2	σ, mb
1	1953	E.B.Paul	14.5	1722	465		1.0010		1724
2	1958	V.J.Ashby	14.1	2520	190	$^{238}U(n,f)$	1.0060		2535
3	1961	R.J.Prestwood	14.81	2356	118	$^{238}U(n,f)$	0.9890		2330
4	1968	W.Dilg	14.7	2320	180	$^{27}Al(n,\alpha)$	1.0000		2320
5	1972	G.N.Maslov	14.2	2243	160	$^{65}Cu(n,2n)$	1.0050	0.9964	2246
6	1972	D.S.Mather	14.3	2578	170	$^{238}U(n,f)$	1.0040		2588
7	1972	A.K.Hankla	14.4	1986	150	$^{27}Al(n,\alpha)$	1.0030		1992
8	1972	D.R.Nethaway	14.43	2168	100	$^{27}Al(n,\alpha)$	1.0024	1.0074	2189
9	1975	B.P.Bayhurst	14.89	2116	89	$^{27}Al(n,\alpha)$	0.9981		2112
10	1975	A.Paulsen	14.8	1890	105	$^{27}Al(n,\alpha)$	0.9990		1888
11	1977	L.R.Veeser	14.7	2064	125	H(n,n)H	1.0000		2064
12	1978	P.Andersson	14.9	2295	116	H(n,n)H	0.9980		2290
13	1980	J.Frehaut	14.76	1935	155	$^{238}U(n,f)$	0.9994		1933
14	1981	T.B.Ryves	14.68	2187	142	$^{56}Fe(n,p)$	1.0002	0.9940	2186
15	1982	J.Csikai	14.66	2087	142	$^{27}Al(n,\alpha)$	1.0004		2088
16	1983	S.Daroczy	8.9~9.9			$^{56}Fe(n,p)$			
17	1983	I.Garlea	14.75	2071	93	$^{235}U(n,f)$	0.9995		2070
18	1984	Y.Ikeda	14.66	2120	110	$^{27}Al(n,\alpha)$	1.0004		2121
19	1985	L.R.Greenwood	14.8	2171	133	$^{93}Nb(n,2n)$	0.9990	0.9905	2148
20	1988	K.Kobayashi	15.0	2125	75	$^{27}Al(n,\alpha)$	0.9980		2120
21	1989	Wang Xiuyuan	14.63	2133	151	$^{27}Al(n,\alpha)$	1.0006	1.0035	2142
22	1989	Lu Hanlin	14.6	2129	95	$^{27}Al(n,\alpha)$	1.0010	1.000	2131

R_1 : Adjusted factor for neutron energy.

R_2 : Adjusted factor for relevant cross section,half-life and gamma branching.

Evaluated Cross Section for 14.7 MeV, Present Work : 2133 ± 34 mb

Lu Hanlin et al : 2137 ± 40 mb, Ryves et al : 2127 ± 26 mb

ENDF / B-6 : 2187.9 mb

References

[1] E. B. Paul et al., EXFOR 11274095
[2] V. J. Ashby et al., Phys. Rev., 111, 616(1958)
[3] R. J. Prestwood et al., Phys. Rev., 121, 1438(1961)
[4] W. Dilg et al., Nucl. Phys., A118, 9(1968)
[5] G. N. Maslov et al., EXFOR 40136020
[6] D. S. Mather, AWRE–0–72 / 72(1972)
[7] A. K. Hankla et al., Nucl. Phys., A180, 157(1972)
[8] D. R. Nethaway., Nucl. Phys., A190, 635(1972)
[9] B. P. Bayhurst et al., Phys. Rev., C12, 451(1975)
[10] A. Paulsen, EXFOR 20486005
[11] L. R. Veeser et al., Phys. Rev., C16, 1792(1977)
[12] P. Andersson et al., LUNF–D6–3021 (1978)
[13] J. Frehaut, EXFOR 20416019
[14] T. B. Ryves et al., NEANDC(E)–212, p. 87(1980)
[15] J. Csikai, Nuclear Data for Science and Technology, Antwerp, 414(1982)
[16] S. Daroczy et al., EXFOR 30814004
[17] I. Garlea et al., INDC(ROM)–15(1983)
[18] Y. Ikeda et al., EXFOR 21945005
[19] L. R. Greenwood, DOE–ER–0046–21, 15(1985)
[20] K. Kobayashi et al., Nuclear Data for Science and Technology, Mito, 261(1988)
[21] Wang Xiuyuan et al., EXFOR 30935007
[22] Zhao Wenrong et al., INDC(CRP)–16 (1989)
[23] Shen Qingbiao et al., CNDP, No. 11, 28(1994)

CNPS01861

IV MULTIGROUP CONSTANT GENERATING AND BENCHMARK TESTING

A Multigroup Constant Library CL50G for Fast Reactor

Liu Guisheng Liu Ping

(Chinese Nuclear Data Center, IAE)

Abstract

The CL50G means CNDC Library of 50 Groups. It is generated through adjusting L50G library which was generated by NJOY-89.31 from ENDF / B-6 and JEF-1. The CL50G library includes 52 nuclides and will be used for fast reactor design calculations in China. Its energy structure is the same as those of LIB-IV 50 group Library given by LANL of U. S. A..

In order to test the reliability of the L50G library, the PASC-1 code system was used for calculating 9 homogeneous and 14 heterogeneous critical fast benchmark assemblies with P_3S_{32} and P_3S_8, respectively. These benchmark assemblies are recommended by CSEWG of the USA. The original calculated results are not good.Although the K_{eff} values for 9 homogeneous assemblies are in agreement with the experimental values, the values for 14 heterogeneous assemblies are too high. On the other hand, F28 (ratio of ^{238}U fission rate to ^{235}U fission rate) values are overpredicted strikingly, too.

Through analyses, it is found that the elastic scattering cross sections in the high energy region are overestimated. We have further known that the structure material nuclides, for example, iron, chromium and nickel have a complicated resonance structures from 0.3 to 5 MeV, but there are no resonance parameters in the File 2 of the evaluated nuclear data libraries, such as ENDF / B-6, JEF-1, JENDL-3 and CENDL-2. Consequently, self-shielding effects in high energy region for these structure material nuclides can not be calculated using

the PASC−1 code system. In other words, the scattering cross sections for these nuclides in high energy region are overestimated. Therefore the L50G library should be adjusted.

As usual, sensitivity analysis code is applied to data adjustment calculations. It is possible that bad calculation result is obtained with the adjusted cross section data owing to the limitation of input integral experimental data. For example, the K_{eff} value from Japanese calculations for ZEBRA−2 with the adjusted multigroup library J3TR1 is worse than the non−adjusted J3T.

In order to avoid the limitation of adjustment, we make the multigroup data adjustment within the range given by the several evaluated microscopic cross sections. The elastic scattering cross sections above 0.82 MeV for iron, chromium and nickel are decreased by 5 %. The ν values, fission and capture cross sections for ^{235}U, ^{238}U and ^{239}Pu are modified a little. Compared with others, all of calculated results with the CL50G are good.

Table 1 K_{eff} values for fast benchmark assemblies

Assembly	C N D C				Caro		JNDC[△]
	L50G	CL50G	B-4	B-6	JEF-1	JEF-2	JENDL-3
JEZEBEL-23	0.99420	0.99349		0.9929	0.9920	0.9756	1.0206
FLATTOP-23	1.00690	0.99307		1.0026	0.9766	0.9836	1.0175
THOR	1.00484	1.00603		1.0056	0.9923	0.9797	0.9985
JEZEBEL	0.99765	0.99944		0.9960	1.0095	0.9952	1.0001
JEZEBEL-Pu	0.99863	0.99999		0.9893	1.0024	0.9898	0.9963
FLATTOP-Pu	0.99326	0.99020		1.0025	1.0054	0.9887	0.9974
GODIVA	0.99979	0.99908		0.9954	0.9995	0.9934	1.0066
FLATTOP-25	0.99909	0.99497		1.0007	0.9984	0.9898	1.0033
BIG-10*	1.00895	0.99601		1.0063	1.0016	0.9928	1.0038
						JENDL-3[△]*	
						J3T	J3TR1
ZPR-3-6F	1.01094	0.99900	1.01389			1.02644	0.99855
ZPR-3-12	1.01630	1.00155	1.01467			1.01451	0.99291
ZPR-3-11	1.01283	0.99871	1.00682			1.01271	0.99369
ZEBRA-2	1.01765	1.00177	0.99367			0.99777	0.97657
ZPR-6-6A	1.02015	0.99706	0.99078			1.00916	0.98626
SNEAK-7A	1.01470	1.00356	0.99967			0.99581	0.99750
ZPR-3-54	1.05283	1.00302	0.96200**			0.96287	0.96460
SNEAK-7B	1.01208	0.99672	0.99570			0.99201	0.99520
ZPR-3-50	1.01564	1.00403	0.98982			0.99584	0.99865
ZPR-3-48	1.01601	1.00107	0.99897			0.99636	1.00027
ZPR-3-49	1.01652	1.00102	1.00110			0.99633	1.00066
ZPR-3-56B	1.02137	1.00392	0.98506			0.99687	0.99876
ZPR-9-31*		0.99808					
ZPR-6-7	1.01608	0.99615	0.98697			0.99306	0.99965

* The measured value for K_{eff} of BIG-10 is equal to 0.996 ± 0.001. All of others are 1.0.

** Quoted from Nuc. Sci. and Eng., Vol. 57, No. 3, July 1975.

△ Quoted from JAERI-M 91-032, p. 148, March 1991.

△* Quoted from JAERI-M 89-026, p. 90, March 1989.

Table 2 Central reaction rate ratios for fast benchmark assemblies

Assembly		Experiment	CNDC		Caro	
			CL50G	B-6	JEF-1	JEF-2
JEZEBEL-23	F28	0.2131	0.9771	1.0081	0.9193	0.9348
	F37	0.9770	0.9905	1.0079	0.9184	0.9393
FLATTOP-23	F28	0.1910	0.9676	1.0030	0.9178	0.9384
	F37	0.8900	0.9919	1.0184	0.9224	0.9483
THOR	F28	0.1950	0.9241	0.9559	0.9990	0.9781
	C28	0.0830	0.8583	0.8500	0.8048	0.8301
	F37	0.9200	0.9416	0.9580	0.9635	0.9633
JEZEBEL	F28	0.2137	0.9298	0.9600	0.9757	0.9528
	F49	1.4480	0.9785	0.9836	0.9878	0.9893
	F37	0.9620	0.9720	0.9889	0.9634	0.9624
	F23	1.578	0.9844	1.0005	0.9185	0.9659
JEZEBEL-Pu	F28	0.2060	0.9358	0.9675	0.9811	0.9651
	F37	0.9200	0.9986	1.0169	0.9859	0.9903
FLATTOP-Pu	F28	0.1800	0.9359	0.9730	0.9844	0.9734
	F37	0.8400	0.9743	1.0042	0.9600	0.9766
GODIVA	F28	0.1647	1.0228	0.9541	1.0595	0.9535
	F49	1.402	0.9912	0.9860	1.0076	0.9922
	F37	0.8370	1.0377	0.9742	1.0167	0.9609
	F23	1.590	0.9851	1.0016	0.9515	0.9676
FLATTOP-25	F28	0.1490	1.0230	0.9655	1.0617	0.9708
	F49	1.370	0.9945	0.9936	1.0126	0.9983
	F37	0.7600	1.0512	1.0016	1.0305	0.9868
	F23	1.600	0.9788	0.9949	0.9476	0.9621
BIG-10	F28	0.0373	1.0078	1.0519	1.0322	1.0142
	C28	0.1100	1.0010	0.9836	1.0145	0.9998
	F49	1.1850	0.9720	0.9985	1.0012	0.9872
	F37	0.3160	0.9823	1.0724	0.9487	0.9720
	F23	1.5800	0.9800	0.9972	0.9691	0.9773

Table 2 Central reaction rate ratios for fast benchmark assemblies (continue)

Assembly	Experiment		CNDC CL50G	HEDL B-4	JAERI J3TR1
ZPR-3-6F	F28	0.0780	1.0087	1.000	1.030
	C28	0.1040	0.9538	0.919	0.990
	F49	1.220	1.0128	1.020	1.018
	F40	0.530	1.0221		
	F23	1.530	1.0153		
ZPR-3-12	F28	0.047	1.0585	1.060	1.105
	C28	0.123	0.9834	0.954	1.002
	F49	1.120	0.9782	0.996	0.995
ZPR-3-11	F28	0.038	1.0187	1.064	1.110
	C28	0.112	0.9911	0.949	1.023
	F49	1.190	0.9671	0.987	0.976
	F40	0.340	1.0209	1.065	
	F23	1.530	1.0105		
ZEBRA-2	F28	0.032	1.0341	1.048	1.102
	C28	0.136	0.9539	0.968	0.990
	F49	0.987	0.9872	1.007	1.015
ZPR-7-6A	F28	0.0241	0.9850	0.926	1.050
	C28	0.1378	1.0190	1.017	1.045
SNEAK-7A	F28	0.0448	0.9574	0.911	1.042
	C28	0.1376	0.9813	0.979	0.985
	F49	1.0160	0.9499	0.960	0.984
ZPR-3-54	F28	0.0254	1.1961	1.176	1.320
	F49	0.9280	0.9286	0.936	0.964
SNEAK-7B	F28	0.0330	1.0048	0.967	1.100
	C28	0.1312	1.0252	1.025	0.985
	F49	1.0120	0.9689	0.985	0.984
ZPR-3-50	F28	0.0251	1.1673	1.132	1.260
	F49	0.9030	0.9771	0.986	1.015
ZPR-3-48	F28	0.0326	1.0426	1.026	1.102
	C28	0.1385	0.9689	0.963	0.980
	F49	0.9760	0.9753	0.993	1.024
ZPR-3-49	F28	0.0345	1.0655	1.055	1.172
	F49	0.9860	0.9884	1.008	1.024
ZPR-3-56B	F28	0.0308	0.9740	0.940	1.070
	F49	1.0280	0.9276	0.944	0.963
ZPR-6-7	F28	0.0220	0.9810	0.914	1.010
	C28	0.1320	1.0350	1.044	1.085
	F49	0.9425	0.9513	0.961	0.993

Table 3 K_{eff} values for 1–D models after all corrections applied to calculations

	CL50G	ENDF / B–5					
	CNDC	ANL	BNL	GE	LANL	ORNL	WARD
JEZEBEL	0.99944	1.0070	1.0055	1.0030	1.0058	1.0043	—
ZPR–9–31	0.99308	1.0054	—	1.0100	1.0083	1.0066	1.0146
ZPR–6–7	0.99615	0.9946	—	1.0007	0.9977	1.0000	0.9999
GODIVA	0.99908	0.9967	1.0013	0.9991	0.9981	0.9967	—
ZPR–6–6A	0.99706	0.9862	—	0.9932	0.9897	0.9915	0.9878

Table 4 Calculated–to–experimental reaction rate ratios (C / E)

Benchmark	Experiment	CL50G	ENDF / B–5					
		CNDC	ANL	BNL	GE	LANL	ORNL	WARD
F49 / F25	(^{239}Pu(n,f)) / (^{235}U(n,f))							
JEZEBEL	1.448 +2.0%	0.971	0.974	0.972	0.974	0.972	0.972	—
ZPR–9–31	0.9452+1.3%	1.020	1.065	—	1.063	1.063	1.062	1.081
ZPR–6–7	0.9422+2.0%	0.951	0.985	—	0.983	0.985	0.983	0.991
GODIVA	1.402 +1.8%	0.991	0.996	—	0.991	0.994	0.996	—
F28 / F25	(^{238}U(n,f)) / (^{235}U(n,f))							
JEZEBEL	.2137 +1.1%	0.930	0.920	0.914	—	0.917	0.917	—
ZPR–9–31	.02836+1.3%	1.024	1.064	—	1.077	1.058	1.062	1.081
ZPR–6–7	.02202+2.0%	0.981	0.987	—	1.002	0.993	0.987	0.986
GODIVA	.1647 +1.1%	1.023	1.036	1.030	—	1.036	1.039	—
ZPR–6–6A	.02411+3.0%	0.985	0.982	—	0.983	0.986	0.977	0.972
C28 / F25	(^{238}U(n,γ)) / (^{235}U(n,f))							
ZPR–9–31	.1163+1.5%	1.101	1.107	—	1.115	1.100	1.100	1.123
ZPR–6–7	.1320+2.0%	1.035	1.058	—	1.061	1.057	1.047	1.076
ZPR–6–6A	.1378+3.0%	1.019	1.038	—	1.042	1.036	1.031	1.051

CNPS01862

A Data Processing and Critical Safety Analyzing Code System NJOY–WIMS

Zhang Baocheng Liu Guisheng Liu Ping Wang Yaoqing

(Chinese Nuclear Data Center, IAE)

Abstract

Based on implements of NJOY, WIMSR, WIMS, modifying WIMSR and compiling SCN and CCMIT, the NJOY–WIMS code system is formed. With this code system, the processing from group constants generating to critical calculations can be done automatically. This is a useful system for updating 69–group WIMS library and benchmark testing for CENDL–2. The results of TRX–1, 2, BAPL–UO_2–1, 2, 3, based on JEF–1 data, from this system have proved that it is reliable and convenient.

Introduction

NJOY[1] is a very famous code system for group constant generation, which can rade the data in ENDF / B–4~ 6 format and have many interface modules. The new version of NJOY includes WIMSR module, which changes GROUPR output into WIMS format group–constant library. WIMS[2] is a general lattice cell programmer, which has been widely used in our country. But the associated 69–group library, released earlier, is very old (based on ENDF / B–4 data). As releasing of ENDF / B–6, BROND–2, JENDL–3.1, CENDL–2 and JEF–1, it becomes necessary to update WIMS library. In 1990, IAEA initiated a WIMS Library Update Project (WLUP)[3]. Due to the definition of data format, up to now, only NJOY code system can be used to generate group constants from ENDF / B–6 format library. Besides, in order to meet the developing trend of nuclear data, Chinese Evaluated Nuclear Data Library Version 2.0 (CENDL–2.0) are presented in the ENDF / B–6 format and Reich–Moore resonance parameters are used in resolved resonance region. NJOY–WIMS can suit for processing CENDL–2 and benchmark testing.

1 NJOY–WIMS Code System

NJOY–WIMS code system consists of NJOY (containing WIMSR module), SCN, CCMIT, and WIMS. In this system, WIMSR module and WIMS code have been improved.

Because only part files of WIMS library can be given with previous WIMSR, and there is a little difference in the order and format between WIMSR output and original library, a great changes were made for WIMSR. At first we added the default files in output, which include general information, energy group–construct, fission source spectrum and burnup data, and deleted useless file. Then $P1$ scattering data were changed from condensed matrix into square one. Through modification, all the files of standard WIMS library can be generated with NJOY.

When WIMS code is used in critical safety analysis, it is necessary to calculate $\bar{\nu}$ from $\bar{\nu}\sigma_f$ and σ_f with formula $\bar{\nu} = \bar{\nu}\sigma_f / \sigma_f$. Clearly, overflow will happen as long as $\sigma_f = 0$ in some energy group, for example ^{238}U. According to the use of $\bar{\nu}$ value, $\bar{\nu}$ was defined as 2.45 when $\sigma_f = 0$. After that, there was no effect on the results and overflow can be escaped.

The processing flow chart of NJOY–WIMS code system is shown in Fig. 1. SCN is a code to select nuclides and collapse libraries. It can receive both binary and BCD data, and can also output binary and BCD data. It can collapse 20 libraries or select 200 nuclides once. Besides, it can change nuclide identification. Many manual work can be replaced by running the code SCN, and all the processing can be done automatically.

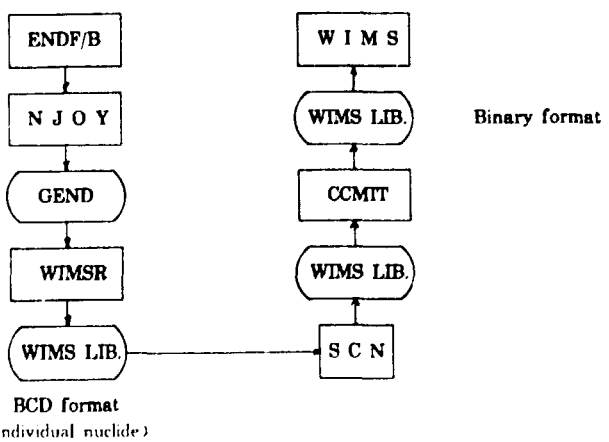

The flow chart of NJOY–WIMS code system treatment

CCMIT is a code to convert BCD format into binary format for WIMS library, and vice versa. WIMS code receives binary data only.

The input cards of SCN and CCMIT are very simple. So the code system is convenient to user.

2 Benchmark Calculations Using NJOY–WIMS Code System

In order to test NJOY–WIMS code system, Benchmark calculations have been done. The selected benchmark lattices include TRX–1, 2, BAPL–UO_2–1, 2, 3. Brief characteristics of the lattices are summarized in Table 1.

Table 1 Brief characteristics for benchmark lattices

Lattice	Fuel	Cladding	Moderator	Fuel Radius (cm)	Pitch (cm)
TRX–1	1.3% enriched U–metal	Al	H_2O	0.4915	1.8060
TRX–2		Al	H_2O	0.4915	2.1740
BAPL–1	1.3% enriched UO_2	Al	H_2O	0.4864	1.5578
BAPL–2		Al	H_2O	0.4864	1.6523
BAPL–3		Al	H_2O	0.4864	1.8057

The following integral parameters besides k–effective were measured at the center of each lattices :

ρ^{28}— the epithermal to thermal ratio of ^{238}U capture.
δ^{25}— the epithermal to thermal ratio of ^{235}U fission.
δ^{28}— the ratio of ^{238}U fission to ^{235}U fission.
C^* — the ratio of ^{238}U capture to ^{235}U fission.

All parameters correspond to thermal cut–off energy of 0.625 eV.

In present calculations, 69–group WIMS library was generated based on JEF–1 data. For WIMS library the fission spectrum was generated by mixed ^{235}U and ^{238}U fission spectrum. To five benchmark experiments mentioned above, the averaged $(\nu\sigma_f)_{238}/(\nu\sigma_f)_{235+238}$ is about 0.075. So the final fission spectrum composed of 7.5% ^{238}U and 92.5% ^{235}U fission spectrum. In the group averaging, CPM spectrum was used for weighting. Cell calculations were made with WIMS / D4 code, and the cylindrical cell approximations were

used to simplify the geometry of the cell. WIMS / D4 uses transport theory to calculate flux as function of the energy and position in the cell. The discrete ordinates method with eight discrete angular distributions was used to solve transport equation, and leakage was treated by the Benoist and B1 method.

3 Results and Discussion

The critical experiments were analyzed using measured bucklings as input. To find the effect of fission spectrum, calculations were done with different fission spectrum (^{235}U, ^{238}U and mixed fission spectrum). The results are shown in Table 2. It is obvious that fission spectrum affect the integral parameters strongly, especially to δ^{28}, because fission of ^{238}U occurs only in high energy. From the Table, it can be seen that the result from mixed fission spectrum is well in agreement with ^{235}U's, and much different from ^{238}U. Of course, it is impossible to use ^{238}U fission spectrum in WIMS library, because only 7.5% fission neutron comes from ^{238}U contribution.

Table 2 Comparison of the results from different fission spectra

	Parameter	Experiment	Calculation With		
			Mixed[a] fiss. spect.	^{235}U fiss. spect.	^{238}U fiss. spect.
TRX-1	K_{eff}	1.0000	0.9952	0.9952	0.9959
	ρ^{28}	1.320 ± .021	1.3531	1.3534	1.3512
	δ^{25}	0.0987 ± .0010	0.09907	0.09907	0.09900
	δ^{28}	0.0946 ± .0041	0.09826	0.09837	0.09659
	C^*	0.797 ± .008	0.7971	0.7972	0.7965
TRX-2	K_{eff}	1.0000	0.9972	0.9972	0.9979
	ρ^{28}	0.837 ± .016	0.8463	0.8464	0.8450
	δ^{25}	0.0614 ± .0008	0.06073	0.06074	0.06069
	δ^{28}	0.0693 ± .0035	0.06978	0.06985	0.06863
	C^*	0.647 ± .006	0.6424	0.6424	0.6420
BAPL-1	K_{eff}	1.0000 ± .00065	1.0020	1.0020	1.0025
	ρ^{28}	1.39 ± .01	1.3857	1.3858	1.3841
	δ^{25}	0.084 ± .002	0.08290	0.08290	0.08284
	δ^{28}	0.078 ± .004	0.07559	0.07567	0.07434
	C^*	——	0.8022	0.8022	0.8017
BAPL-2	K_{eff}	1.0000 ± .00062	1.0014	1.0014	1.0020
	ρ^{28}	1.12 ± .01	1.1538	1.1539	1.1525
	δ^{25}	0.068 ± .001	0.06763	0.06763	0.06758
	δ^{28}	0.070 ± .004	0.06507	0.06514	0.06401
	C^*	——	0.7318	0.7318	0.7313
BAPL-3	K_{eff}	1.0000 ± .0005	1.0014	1.0014	1.0020
	ρ^{28}	0.906 ± .010	0.9070	0.9071	0.9060
	δ^{25}	0.052 ± .001	0.05198	0.05198	0.05195
	δ^{28}	0.057 ± .003	0.05341	0.05346	0.05257
	C^*	——	0.6548	0.06548	0.6545

a) Mixed by 92.5% ^{235}U and 7.5% ^{238}U fission spectrum.

Table 3 Comparison of results between calculations and measurements

	Parameter	Experiment	Calculations		
			N–W[b] by CNDC	WIMS from ref.4	WIMS with old lib.
TRX–1	K_{eff}	1.0000	0.9952	0.9996	1.0023
	ρ^{28}	1.320 ± .021	1.3531	1.336	1.279
	δ^{25}	0.0987 ± .0010	0.09907	0.0988	0.0990
	δ^{28}	0.0946 ± .0041	0.09826	0.0978	0.0965
	C^*	0.797 ± .008	0.7971	0.793	0.780
TRX–2	K_{eff}	1.0000	0.9972	0.9984	0.9965
	ρ^{28}	0.837 ± .016	0.8463	0.842	0.808
	δ^{25}	0.0614 ± .0008	0.06073	0.0608	0.0610
	δ^{28}	0.0693 ± .0035	0.06978	0.0699	0.0695
	C^*	0.647 ± .006	0.6424	0.643	0.636
BAPL–1	K_{eff}	1.0000 ± .00065	1.0020	1.0057	1.0029
	ρ^{28}	1.39 ± .01	1.3857	1.385	1.358
	δ^{25}	0.084 ± .002	0.08290	0.0832	0.0840
	δ^{28}	0.078 ± .004	0.07559	0.0758	0.0755
	C^*	——	0.8022	0.803	0.800
BAPL–2	K_{eff}	1.0000 ± .00062	1.0014	1.0043	1.0005
	ρ^{28}	1.12 ± .01	1.1538	1.156	1.133
	δ^{25}	0.068 ± .001	0.06763	0.0679	0.0687
	δ^{28}	0.070 ± .004	0.06507	0.0653	0.0652
	C^*	——	0.7318	0.734	0.732
BAPL–3	K_{eff}	1.0000 ± .0005	1.0014	1.0034	0.9981
	ρ^{28}	0.906 ± .010	0.9070	0.911	0.894
	δ^{25}	0.052 ± .001	0.05198	0.0523	0.0529
	δ^{28}	0.057 ± .003	0.05341	0.0536	0.0538
	C^*	——	0.6548	0.0657	0.657

b) N–W stands for NJOY–WIMS code system

The comparison of the results between calculations and measurements is shown in Table 3. The calculated integral parameters by CNDC are close to the experiments and results of IAEA[4], and much better than that from old WIMS library. According to the results we can say that the NJOY–WIMS code system

is reliable and it can be used to update WIMS library. By the way, the benchmark testing for CENDL–2 can be done with this code system.

References

[1] NJOY91.91 : A Code System for Producing Pointwise and Multigroup Neutron and Photon Cross Sections From ENDF / B Evaluated Nuclear Data. PSR–171, Radiation Shielding Information Center, USA, Oct., 1993

[2] M. J. Halsall, A Summary of WIMS / D4 Input Options. AEEW–M1327, July 1980

[3] S. Ganesan, Invitation Letter to Participate in the WIMS Library Update Project, IAEA, Nov. 15, 1990

[4] A. Trkov, M. Ravink, WIMS Library Update Project. Final Report on Stage 2, IJS–DP–6726 (1993)

CNPS0163

Benchmark Testing of Total Cross Section for Fe, O, Na, N

Liu Ping

(Chinese Nuclear Data Center, IAE)

Introduction

When neutron beams from source (reactor) pass through the collimator, and transmit the sample, some neutrons change the direction through the neutron scatter, some neutrons, which have no any collision in the sample, are detected by the detector. These experiments are called broomstick experiments, which were designed to test neutron total cross sections for nuclides (Fe, O, Na, N) in the energy range 0.8～11.0 MeV[1~4].

1 Method of Calculation

The calculation consists of two steps :

1.1 The calculation of a transmitted uncollided spectrum $N_{unc}(\Delta E')$:

$$N_{unc}(\Delta E') = \sum_{E_i \text{ in } \Delta E'} N_0(E_i) \exp(-\Sigma_{tot}(E_i)\, t)\, \Delta E_i / \Delta E'$$

where t is the thickness of sample, and Σ_{tot} is the macroscopic total cross section of sample. The total number of energy subintervals ΔE_i, which used in the range 0.5~ 12.0 MeV, are taken from Refs. [1]~ [4], $N_0(E_i)$, which is given in the Refs. [1]~ [4], is the source spectrum and $N_0(E_i)$ is taken or interpolated in the following formula :

$$N_0(E) = ((E_2-E)/(E_2-E_1))\, N_0(E_1) + ((E-E_1)/(E_2-E_1))\, N_0(E_2)$$

1.2 The Calculation of $N_{unc}(E)$:

$$N_{unc}(E) = \sum_{E'} N_{unc}(\Delta E')\, R(E' \to E)\, \Delta E'$$

$R(E' \to E)$ is a Gaussian function at E', and

$$R(E' \to E) = (93.944/aE') \exp - [((((E'-E)\, 235.482)/E'a)^2/2]$$

where a, which is taken from Refs. [1]~[4], is interpolated in the following formula :

$$a(E) = (E_2-E)/(E_2-E_1)\, a(E_1) + (E-E_1)/(E_2-E_1)\, a(E_2)$$

2 Additional Explanation

Because there is oxygen in the water, it must affect the result of oxygen's $N_{unc}(E)$, so we should correct the transmitted spectrum by given correction factors. They are given in Ref. [2].

3 Code

According to the formula mentioned above, we updated two codes — GETMT1 and FEONAN, which were developed by Dr. Yu Peihua. GETMT1 can read the total cross section from an ENDF / B tape, and outputs the total

cross section in the range 500 keV~12 MeV. FEONAN can calculate uncollided flux, and smooth the uncollided flux with the resolution function of the spectrometer system, and outputs the flux after smoothing in the energy grid.

4 Result and Comparison

The GETMT1 and FEONAN codes are used to calculate four nuclides (iron, oxygen, sodium, nitrogen) with different evaluated nuclear data (CENDL-2, JEF-1, JENDL-3, ENDF / B-6). The calculated results for each nuclide from those libraries are compared with each other. The results of CENDL-2 are compared with the experimental values[1~4].

4.1 Iron

In 0.8~11.0 MeV range, the result of iron from different libraries are compared in Figs. 1~4, where, above 3 MeV, CENDL-2.0 and CENDL-2.1 are close to experiment and other libraries. Below 3 MeV, CENDL-2.0 is smaller than experiment and other libraries, but CENDL-2.1 is more close to experiment than CENDL-2.0, and ENDF / B-6 is higher than other libraries. The difference between iron1 and iron2 is the different thickness of iron sample.

4.2 Oxygen

In 1.9~8.6 MeV range, the comparisons for oxygen are described in Figs. 5, 6, where CENDL-2 is the same value as JENDL-3 and ENDF / B-6 in whole energy range, they are all higher than experiment in the energy range 2.3 ~2.5 MeV, and close to experiment in other energy range.

4.3 Sodium

In 0.8~11.0 MeV range, the comparisons for sodium are described in Figs. 7, 8, where, CENDL-2 is close to experiment, and the same value as ENDF / B-6 in the whole energy range. But JENDL-3 is higher than other libraries.

4.4 Nitrogen

The comparison energy range is 0.8~10.0 MeV. In the energy range 0.9~1.2 MeV, 1.6~1.8 MeV, 3.4~4.0 MeV, CENDL-2 is higher than experiment.

CENDL-2 is close to experiment in other energy range. Below 5.5 MeV, CENDL-2 is close to ENDF/B-6 and JENDL-3. Above 5.5 MeV, CENDL-2 is the same value as ENDF/B-6, but JENDL-3 is higher than other libraries. See Figs. 9, 10.

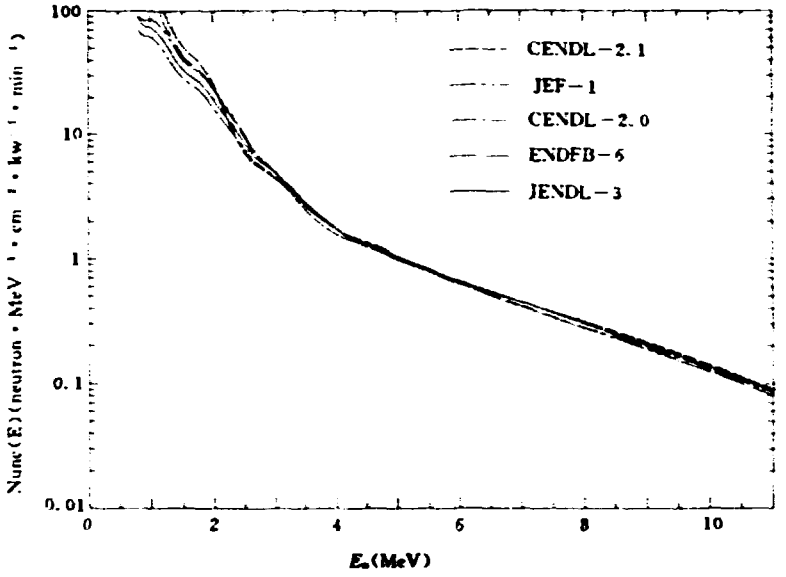

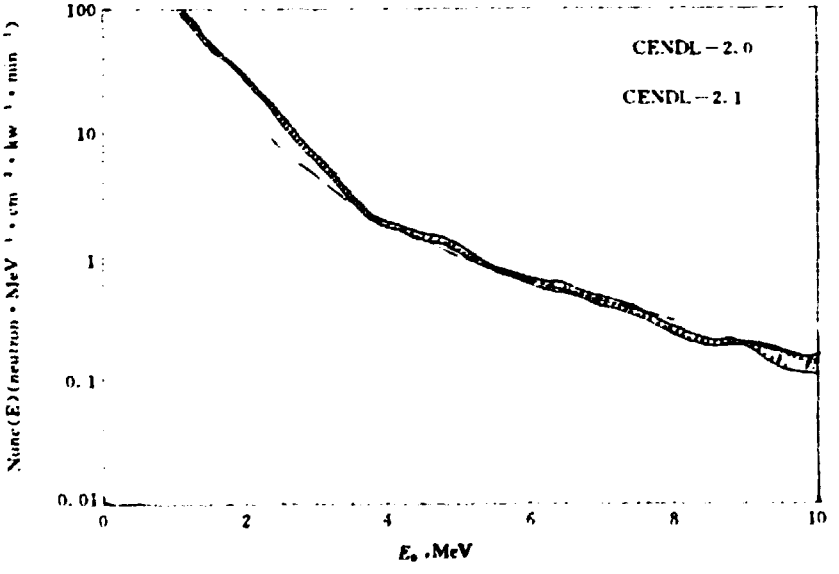

Fig. 1, 2 Transmitted spectrum through iron1

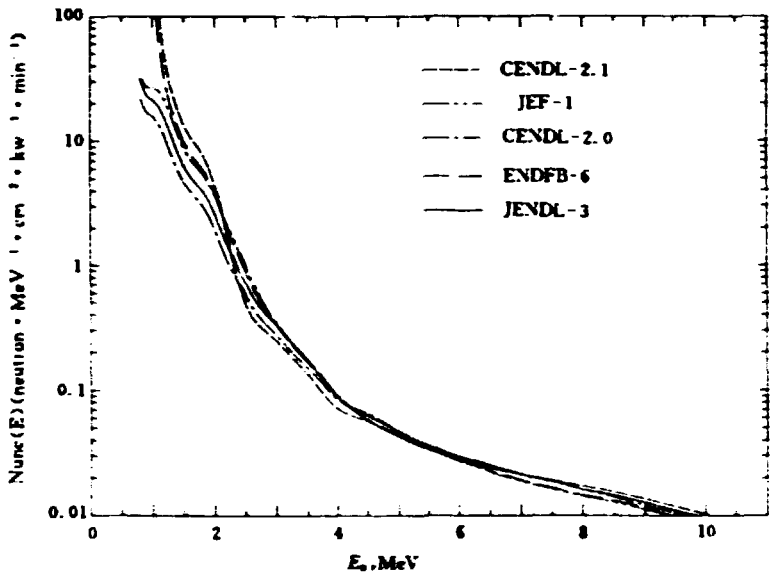

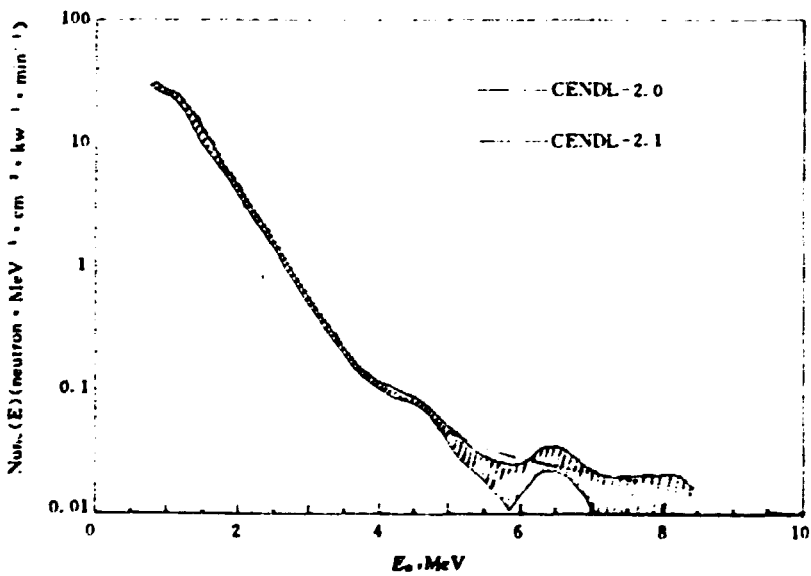

Fig. 3, 4 Transmitted spectrum through iron2

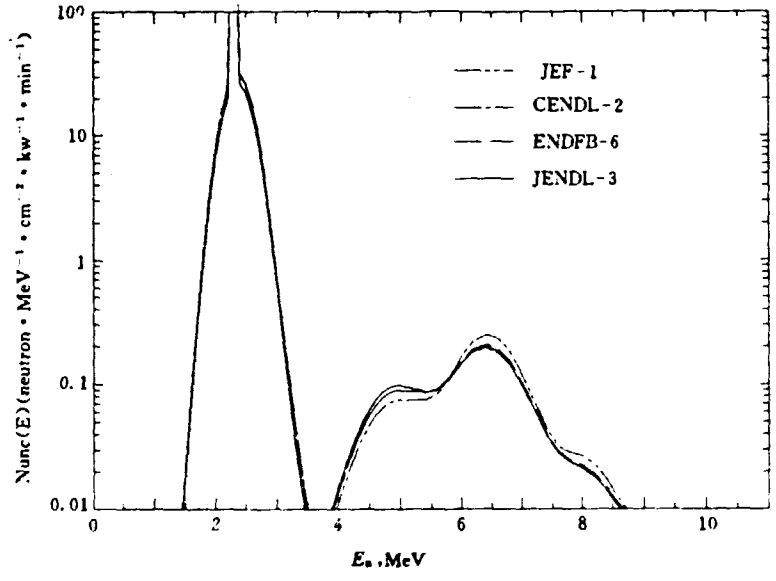

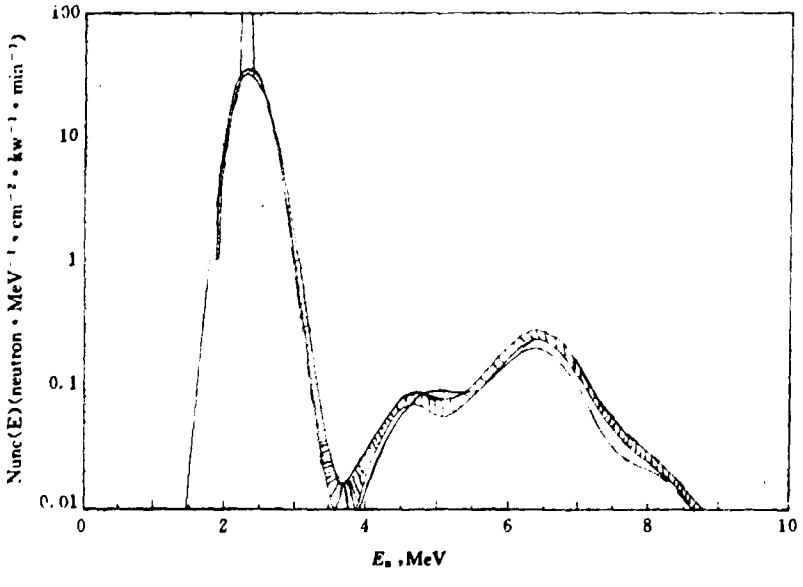

Fig. 5, 6 Transmitted spectrum through oxygen

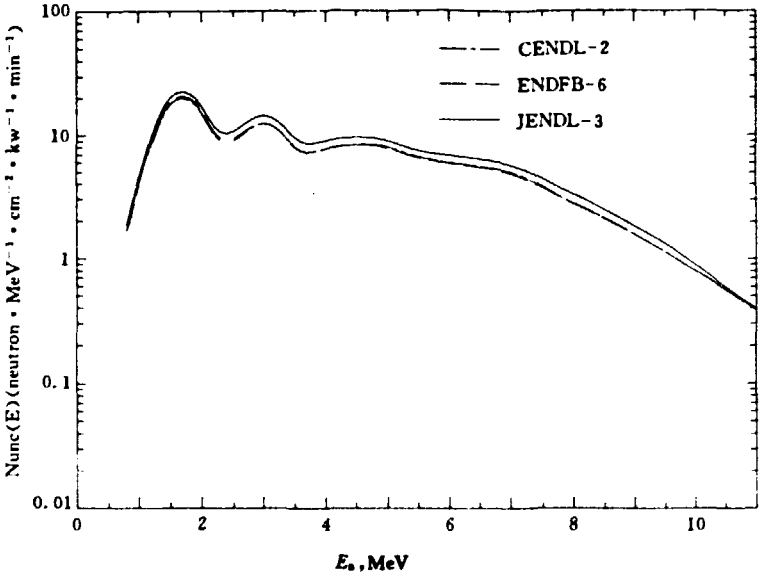

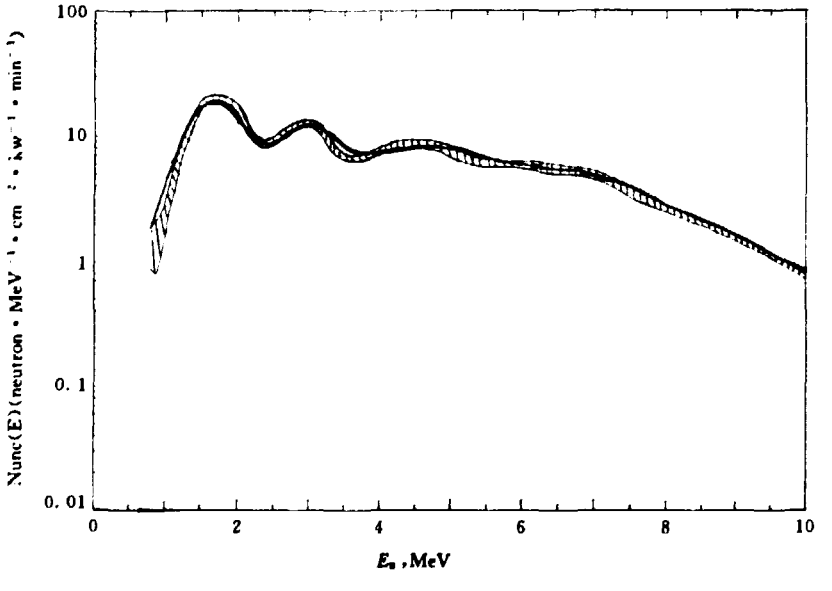

Fig. 7, 8 Transmitted spectrum through sodium

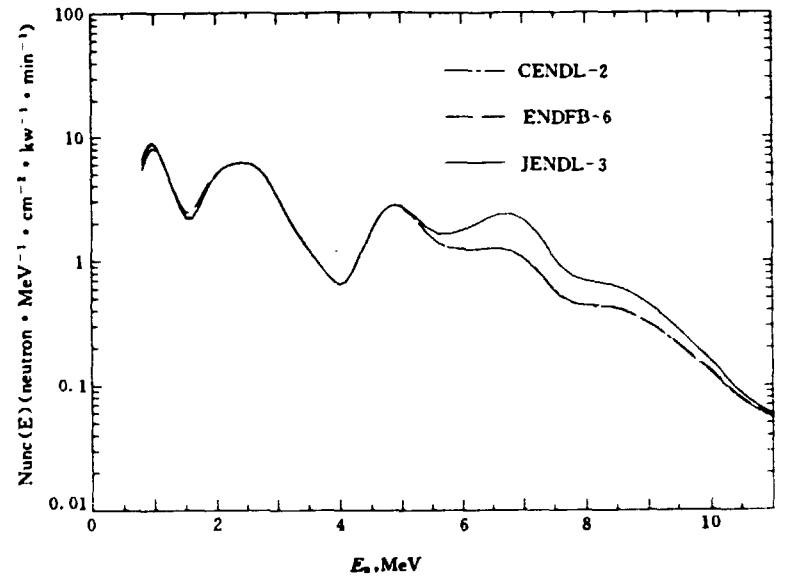

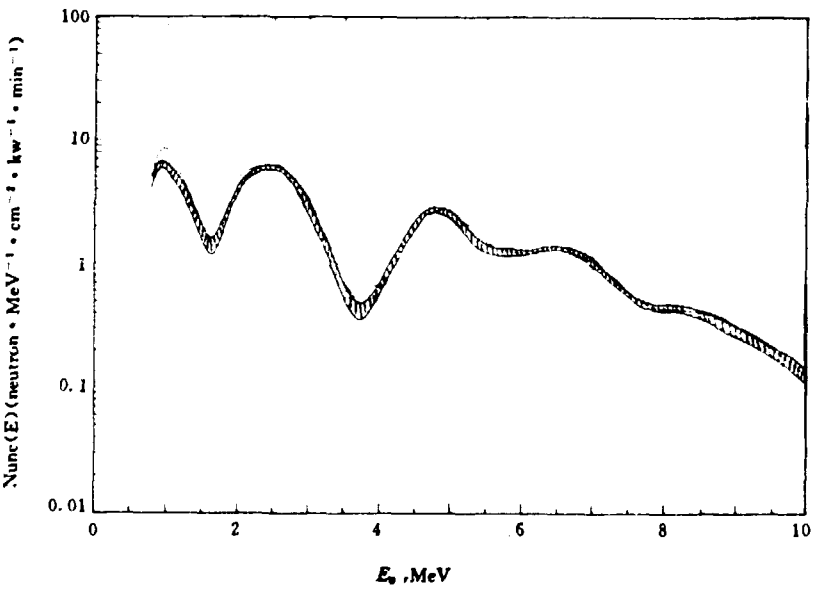

Fig. 9, 10 Transmitted spectrum through nitrogen

References

[1] R. E. Maerker, ORNL-TM-3867 (ENDF-166), September 1972

[2] R. E. Maerker, ORNL-TM-3868 (ENDF-167), September 1972

[3] R. E. Maerker, ORNL-TM-3869 (ENDF-168), September 1972

[4] R. E. Maerker, ORNL-TM-3870 (ENDF-169), September 1972

CNPS01164

V PARAMETER AND PROGRAM LIBRARIES

The Management — Retrieval Code of the Sub-Library of Atomic Mass and Characteristic Constants for Nuclear Ground State

Su Zongdi Ma Lizhen

(Chinese Nuclear Data Center, IAE)

The management-retrieval code of the sub-library of atomic mass and characteristic constants for nuclear ground state (MCC) is used for displaying the basic information on the MCC sub- library on the screen, and retrieving the required data. The retrieved results are put into the data file OUTMCC.DAT. The code was finished at Chinese Nuclear Data Center (CNDC), and has widely been used in nuclear model calculations of nuclear data and other fields.

1 Basic Information

The MCC management-retrieval code could retrieve the following data :

ME : Mass excess ($M-A$). Most of mass excesses are the experimental data, compiled by A. H. Wapstra et al.[1]. An appended "s" denotes that the value is from systematics[1]. An appended "t" denotes that the value is calculated by P. Moller et al.[2].

J, *P* and $T/2$: Spin, parity and half-life of ground state. Most of these values were taken from the Evaluated Nuclear Structure Data File (ENSDF)[3].

AB : Abundance. Taken from Ref. [4].

The others, such as atomic mass M, total binding energy B; separation energies of some particles and particle groups and beta-decay energies; nuclear reaction energy Q and the corresponding threshold energy E_t for some reaction channel up to the third reaction process can also be derived by the combi-

nations of different mass excesses by using this code.

The MCC data file contains the data of 4800 nuclides ranging from $Z = 0$, $A = 1$ to $Z=122$, $A=318$. Most of these data are from the references mentioned above, and a few are collected and complied by us.

2 Retrieval Ways

This code provides two retrieval ways . One is for single nucleus (SN), and another is for a neutron reaction (NR). The latter contains four kinds of retrieval types corresponding to four types of different neutron calculation codes respectively. They are :

1) The first type (FUP code)

1st process	2nd process	3rd process
(n,γ) (Z, A+1)	(n,2n) (Z, A−1)	(n,3n) (Z, A−2)
(n,n) (Z, A)		

2) The second type (emitted particles without d, t, ^{3}He)

1st process	2nd process	3rd process
(n,γ) (Z, A+1)	(n,2n) (Z, A−1)	(n,3n) (Z, A−2)
(n,n) (Z, A)	(n,np) (Z−1, A−1)	(n,2np) (Z−1, A−2)
(n,p) (Z−1, A)	(n,n^{4}He) (Z−2, A−4)	(n,2n^{4}He) (Z−2, A−5)
(n,^{4}He) (Z−2, A−3)	(n,pn) (Z−1, A−1)	
	(n,2p) (Z−2, A−1)	
	(n,p^{4}He) (Z−3, A−4)	
	(n,^{4}He n) (Z−2, A−4)	
	(n,^{4}He p) (Z−3, A−4)	
	(n,2^{4}He) (Z−4, A−7)	

3) The third type (UNF code)

1st process	2nd process	3rd process
(n,γ) (Z, A+1)	(n,2n) (Z, A−1)	(n,3n) (Z, A−2)
(n,n) (Z, A)	(n,np) (Z−1, A−1)	
(n,p) (Z−1, A)	(n,n^{4}He) (Z−2, A−4)	
(n,d) (Z−1, A−1)	(n,pn) (Z−1, A−1)	
(n,t) (Z−1, A−2)	(n,2p) (Z−2, A−1)	
(n,^{3}He) (Z−2, A−2)	(n,^{4}He n) (Z−2, A−4)	
(n,^{4}He) (Z−2, A−3)		

4) The fourth type (MUP code, 49 kinds of channel)

1st process	2nd process	3rd process
(n,γ) (Z, A+1)	(n,nx)	(n,3n) (Z, A−2)
(n,n) (Z, A)	(n,px)	(n,2np) (Z−1, A−1)
(n,p) (Z−1, A)	(n,dx)	(n,2nd) (Z−1, A−3)
(n,d) (Z−1, A−1)	(n,tx)	(n,2nt) (Z−1, A−4)
(n,t) (Z−1, A−2)	(n,^{3}He x)	(n,2n^{3}He) (Z−2, A−4)
(n,^{3}He) (Z−2, A−2)	(n,^{4}He x)	(n,2n^{4}He) (Z−2, A−5)
(n,^{4}He) (Z−2, A−3)	(x = n, p, d, t, ^{3}He, ^{4}He)	

The retrieved results are classified and put into data file "OUTMCC.DAT".

3 Conclusion

The MCC sub−library (Version 1) has been set up at CNDC, and has been used to provide the atomic masses and characteristic constants of nuclear ground states for the nuclear model calculations, nuclear data evaluations and other fields.

There are the mass excesses of 4800 nuclides including exotic nuclei quite far from the stability valley in the MCC data file,therefore this sub−library could satisfy requirements of different users.

It is very simple and convenient to retrieve atomic masses and related data by using the management retrieval code, because of adopting the man–computer interaction and providing various choice.

As the next step, the data of the MCC sub–library, such as *ME* and the data relative to *ME*, will be updated, and the management–retrieval code should further be perfected for wider applications.

Acknowledgment

The authors would like to thank NDS / IAEA and NNDC / BNL for providing us the data tapes with mass excesses, ENSDF and so on.

References

[1] A. H. Wapstra, G. Audi, R. Hoekstra, At. Nucl. Data Tables, 39, 281(1988)

[2] P. Moller, M. J. Swiatecki and J. Treiner, At. Nucl. Data Tables 39, 225(1988)

[3] Evaluated Nuclear Structure Data File, maintained by the National Nuclear Data Center, Brookhaven National Laboratory. (March, 1991)

[4] N. E. Holden, Table of the Isotopes, 71st edition (1990)

CNPSD 1105

Discrete Level Schemes and Their Gamma Radiation Branching Ratios (CENPL–DLS) (I)

Su Zongdi Zhang Limin Zhou Chunmei Sun Zhengjun

(Chinese Nuclear Data Center, IAE)

The DLS data file, which is a sub–library (Version 1) of Chinese Evaluated Nuclear Parameter Library (CENPL), consists of data and information of discrete levels and gamma radiations. The data and information of this data file are translated from the Evaluated Nuclear Structure Data File (ENSDF)[3], which is maintained by the National Nuclear Data Center (NNDC) at Brookhaven National Laboratory based on evaluation from the International

Nuclear Structure and Decay Data Network, coordinated by the IAEA. The transforming code from ENSDF to DLS was written, and the transformation of the data and information was finished. The data have further been checked and corrected, and the levels, which are of undetermined energy, and their gamma radiations were deleted. Finally, the DLS data file has been set up. The data format is suitable for computer reading and listing table.

Contents

In the DLS data file, there are the data on discrete levels with determinate energy and their gamma radiations. For each measured level, its order number, energy, spin, parity and half-life, as well as the order numbers to the final levels, branching ratios and multipolarities for gamma radiations are listed. At present, this file contains the data of 79456 levels and 100411 gammas for 1908 nuclides.

Format

The first line for each nuclide contains :

Z (1～3, the column number, the same below), the charge number; *EL* (4～6), the element symbol; *A* (7～10), the mass number.

The records of the line marked "*L*" in 13 column contain the level data *NL*, *E*, *dE*, *', P*, *IS*, *UL* and *T / 2*, as defined below :

NL (14～16), the order number of level; *E* (17～27), the level energy in keV; *dE* (28～30), the standard uncertainty of *E*; *J*, *P* (31～49), the level spin and parity; *IS* (50), the isomeric state is denoted by "*M*"; *UL* (51), the character "?" denotes an uncertain or questionable level; *T / 2* (66～83), the level half-life.

The records of the line marked "*G*" in 52 column contain the data of the gamma radiation for the level listed above, *NG*, *Br*, *dBr*, *MP* and *UG*, as defined below :

NG (53～55), the order number to final level for gamma transition; *Br* (56～61), the branching ratio or relative photo intensity for gamma radiation; *dBr* (62～ 65), the standard uncertainty of *Br*; *Mp* (66～ 83), the multipolarity of gamma radiation; *UG* (84), the character "?" denotes an uncertain placement of the transition in the level scheme, letter "*s*" denotes an expected, but not yet observed transition.

The project was supported in part by the International Atomic Energy Agency and National Natural Science Foundation of China.

Acknowledgment

The authors would like to thank NNDC, BNL for providing us the data tapes with ENSDF and so on.

Example:

Z EL	A	NL	E	dE	J , P	ISUL	NG	Br	dBr	T/2 or Mp	UG
21 Sc	46	L 1	0.0		4+					83.810 D	10
		L 2	52.011	1	6+					9.4 US	8
							G 1	100.0		E2	
		L 3	142.528	7	1-	M				18.75 S	4
							G 1	100.0		E3	
		L 4	227.767	9	3+					270 PS	LT
							G 1	100.0		M1	
		L 5	280.701	13	5+					270 PS	LT
							G 1	5.8	7	M1	
							G 2	94.2	7	M1	
			.					.			
			.					.			
			.					.			
		L 16	1141	6							
		L 17	1270.46	3	4-						
							G 1	40.6	11		
							G 8	21.2	10	M1	
							G 9	38.2	11	M1	
		L 18	1298	5							
		L 19	1321.12	3	3+,(4+)						
							G 1				
							G 11	100.0		M1	
		L 20	1394.18	4	2+						
							G 3			E1	
							G 4	79.2	13	M1	
							G 13	20.8	13	M1	
		L 21	1427.90	4	(2+)						
							G 3	100.0			
		L 22	1526.74	5	(2-,3,4+)						
							G 7	50.6	19		
							G 8				
							G 9	49.4	19		
			.					.			
			.					.			
			.					.			

Reference

[1] Evaluated Nuclear Structure Data File, maintained by the National Nuclear Data Center, Brookhaven National Laboratory, (File as of 1991)

CNPS01866

Retrieve Codes for User

— Introduction of Program Retrieve

Liu Ruizhe Zhang Limin

(Chinese Nuclear Data Center, IAE)

The current demand to retrieve codes effectively from the Computer Program Library (CPL) has now made it necessary to develop and utilize a new retrieve tool. So the code RETRIEVE is designed and developed.

Every code stored in NEA Data Bank has a abstract which contains seventeen terms. The similar abstracts were written in CNDC for every code developed by either Chinese or foreigners. The contents of the abstract are as follows :

1. Name or designation of program.
2. Computer for which program is designed and other machine version packages available.
3. Description of program or function.
4. Method of solution.
5. Restrictions on the complexity of the problem.
6. Typical running time.
7. Unusual features of the program.
8. Related and auxiliary programs.
9. Status.
10. References.
11. Machine requirements.
12. Programming language used.
13. Operating system under which program is excuted.
14. Other programming or operating information or restrictions.
15. Name and establishment of authors.
16. Material available.
17. Category and keywords.

The code RETRIEVE is excuted under this data environment.

By using the code RETRIEVE, users can retrieve the codes stored in CPL

according to their names, author(s), category and keywords. In CNDC, there are two sublibraries named Chinese program sublibrary and foreign sublibrary.

Correspondently, the abstract files are ABSTRACT.CHA and ABSTRACT.NEA respectively. They are the input of RETRIEVE. The code was written in FORTRAN 77 and is available at CNDC.

CNPSO1867

VI ATOMIC AND MOLECULAR DATA

An Evaluated Data Library for Light Particle Reflections from Solid Surfaces

Yao Jinzhang Fang Shaohong Yu Hongwei

(Chinese Nuclear Data Center, IAE)

Particle reflection from solid surface is important in various fields of research and application including the development of thermonuclear-fusion device. Recent reviews of studies on the reflection are given by E. W. Thomas et al.[1] and W. Eckstein[2]. We present an evaluated data base for light projectiles reflection.

The particle reflection is characterized by two parameters. One is particle number reflection coefficient, R_n, defined as the ratio of reflection particle to all incident particles. Another is energy reflection coefficient, R_e, defined as the energy carried away by the reflected particles divided by the energy of the incident particles.

In a general case, the particle reflection coefficient is high at low energy and decreases monotonically as projectile energy increases. There are some arguments as to how one should describe reflection at vanshingly low energies, if a projectile can be retained in the target (solid surface), then reflection should tend to zero. M. I. Baske gave some calculation results of low energy region from 0.1 to 100 eV by Embeded Atom Method[3] at normal incidence for H^+ and Ni combination. It shows that reflection coefficient decreases to zero as projectile energy from 10 eV down to 0.1 eV. Luo Zhengming et al.[4] calculated particle and energy reflection coefficients of twelve species by various incoming particles with ion-transport bipartition model (i. e revision version of PANDA-P) which considered binding energy of solid surface. The results are given in the figures. A new empirical formula[5] has been used to calculate the reflection coefficients of light particles projected on solid surface at normal incidence. It is shown as

$$R_e = \{ (0.705/f)/[1 + (\varepsilon/0.047)^{0.597} + (\varepsilon/0.619)^{1.5}] \} - \exp [-\pi (M_1 + M_2) \varepsilon]$$

Where $R_n = R_e/\gamma_e$

$$\gamma_e = 1/[1 + (\varepsilon/0.133)^{0.285}] + 0.530/[1 + (\varepsilon/85)^{-1.46}]$$

$$f = F(Z_1, Z_2, M_1, M_2, E_0)$$

Z_1, Z_2, M_1 and M_2 represent the charges and masses of projectile (subscript–1) and target (subscript–2), respectively. E_0 is energy of incident particle.

$$\varepsilon = 0.032534 M_2 E_0 / Z_1 Z_2 (M_1 + M_2) (Z_1^{2/3} + Z_2^{2/3})^{1/2}$$

The experiments are quite few and cover only a limited range of collision species. At low energies (< 10 eV), the particle stripping is very inefficient, so that lowest energy recoils can not be detected.

We have collected numerous reflection experimental data and theoretical calculations up to the end of 1993. The recommended values are given in terms of B–spline function fitting both experimental data and calculated data. A data base on reflection of light particles bombarded on solid surfaces was established in ALADDIN format[6]. As an example, Figs. 1～4 show critical recommended values of particle and energy reflection coefficients for H+ projectile on Fe and Ni targets. In the figures, Emp represents calculated values by revised empirical formula, Luo is the calculation results by Luo Zhengming et al., Exp shows experimental measurements, Rec indicates recommended values.

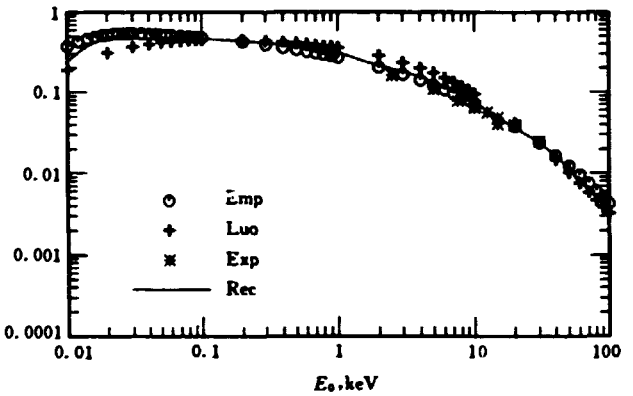

Fig. 1 R_n vs E_0 for H^+ on Fe solid surface

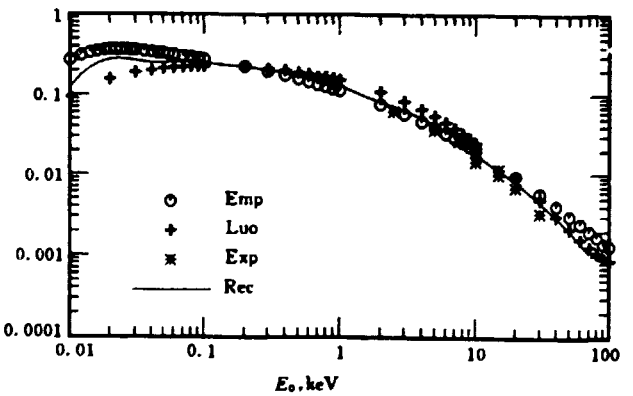

Fig. 2 R_c vs E_0 for H^+ on Fe solid surface

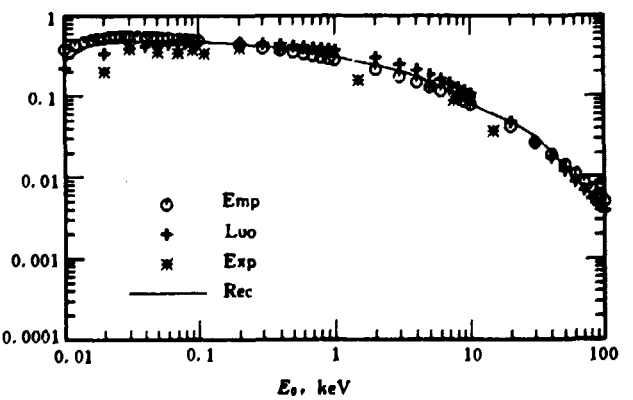

Fig. 3 R_n vs E_0 for H^+ on Ni solid surface

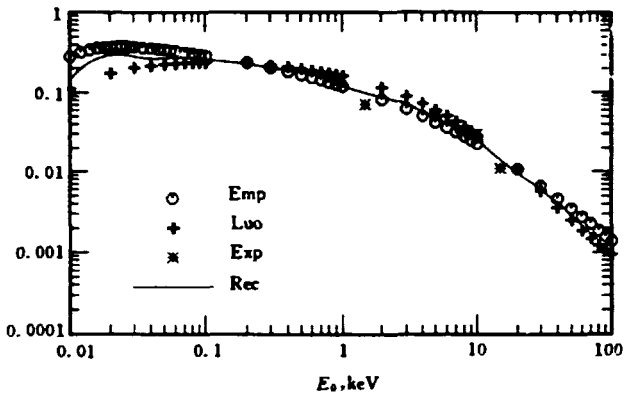

Fig. 4 R_c vs E_0 for H^+ on Ni solid surface

References

[1] E. W. Thomas et al., INDC (NDS)–249 (1991)
[2] W. Eckstein, Nuclear Fusion Supplement, Vol. 1(1991)
[3] M. I. Baskes, Journal of Nuclear Materials, 128 & 129, 676(1984)
[4] Luo Zhengming, Private Communication (1992)
[5] Fang Shaohong et al., Communication of Nuclear Data Progress No. 10, 117(1992)
[6] IAEA–NDS–AM–17 by A+M Unit, IAEA

CNPS0186

Study of Physical Sputtering Systematics

Yu Hongwei Yao Jinzhang

(Chinese Nuclear Data Center, IAE)

Sputtering of solids surfaces is very important for a large number of applications, for instance, the interaction of particle with plasma wall in fusion device will induce the surface etching and produce the impurities. So it is important to understand the physical processes and to obtain reliable sputtering yield data. In our previous work[1], the sputtering yields for carbon and nickel solid

surfaces with H^+, D^+, T^+ and He^+ projectiles at normal incidence were calculated using the formula of Bohdasky[2]. The values calculated are in good agreement with experiments and Monte Carlo calculations. It is a most extensively used empirical formula. We computed further the sputtering yields for many projectile–target combinations from threshold energy to about 100 keV at normal incidence by empirical formula above. The formula is simply described as follows:

$$Y(E,0) = \frac{0.042}{U_s}\left(\frac{R_p}{R}\right)\alpha S_n(E)\left(1-\left(\frac{E_{th}}{E}\right)^{2/3}\right)\left(1-\frac{E_{th}}{E}\right)^2$$

Where E is the projectile energy, $S_n(E)$ is the nuclear stopping cross section, U_s is the binding energy of solid surface, $R/R_p = K\frac{M_2}{M_1}+1$, K is an adjustable parameter, E_{th} is the threshold energy.

The sputtering systematics with variation of energy and mass of projectile and target atomic mass is briefly discussed from results calculated.

1. In general, the sputtering yields increase with incident energy increasing at first, and then decrease with the energy increasing further. As an example, Fig. 1 shows the change of sputtering yields of carbon surface by H^+, D^+, T^+ and He^+ projectiles, the uppermost line is for He^+ projectile and the others follow in descending order for T^+, D^+ and H^+ projectiles, respectively. The reason is that the energy moved from projectile to solid surface atom increase with projectile mass increasing.

2. The peak positions of sputtering yields for various solid targets by same projectile are shifted on the energy axis. They depend on the masses of target atoms. Fig. 2 presents the situation. The position of peak of sputtering locates at the left side of energy axis for lightest target atom, C and others move forward to right for Si, Ni and Au target atoms. It is probably determined by the reaction threshold energy of combination and surface binding energy of solid target.

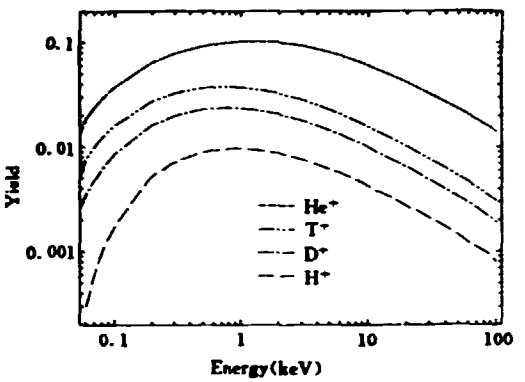

Fig. 1 Sputtering yields of Si by various projectiles

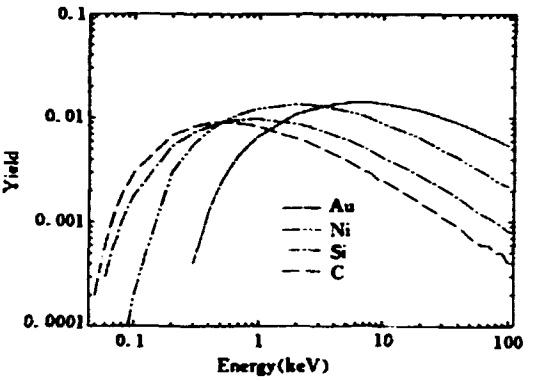

Fig. 2 Sputtering yields of various targets by H^+

References

[1] Yao Jinzhang et al., Communication of Nuclear Data Progress, 10, 112(1993)

[2] Bohdansky, J., Nucl. Instrum. Methods in Phys. Res., B2, 587(1984)

CNPS0186P

VII DATA PROCESSING

Comparison of Two Approximation Methods to Deal with PPP Phenomenon in Practice

Zhao Zhixiang

(Chinese Nuclear Data Center, IAE)

Introduction

During the combination and fitting of derived quantities, people must pay attention to so called PPP phenomenon.In the author's early papers on PPP [1~2], it was demonstrated that PPP phenomenon can be attributed as the inconsistencies in generating derived quantities and their covariance matrix, and that these inconsistencies can be avoided by dealing with the problem in so-called data space or eliminated by an iterating process in derived quantity space. Generally speaking, to deal with derived quantities strictly, we need to know directly measured data and their covariance matrix, from which the derived quantities are obtained, and relationship between derived quantity and directly measured data. Unfortunately, it is usually difficult for an evaluator to know all of information mentioned above. Chiba and Smith proposed an approximation method to be used in practices[3] which is equivalent to the approximation suggested by Zhou[4]. In present paper, Chiba's approximation is derived under some assumptions and the another approximation is also proposed. The comparison of these two approximations is carried out for several examples.

1 Two Approximation Methods

Let us assume that we have two derived quantities Y_1, Y_2 and their reported covariance matrix consisting of $\sigma_R^2(Y_1)$, $\sigma_R^2(Y_2)$, $\mathrm{Cov}_R(Y_1,Y_2)$. As we pointed out[1], if Y_1 and Y_2 were derived from directly measured data from a non-linear relationship, the elements of their covariance matrix would be incorrect. We hope to correct them for obtaining corrected covariance matrix

denoted by $\sigma_C^2(Y_1)$, $\sigma_C^2(Y_2)$ and $\mathrm{Cov}_C(Y_1, Y_2)$.

Assuming that : 1) the deriving relationships for Y_1 and Y_2 are the same; 2) the statistical error of Y_i is mainly introduced by directly measured data a_i and the covariance between Y_1 and Y_2 introduced by C; and 3) Y_i as the function of a_i and C is separative, the deriving relationship can be written as

$$Y_i = f(a_i, C) = \Psi(X_i)\Phi(C) \tag{1}$$

Therefore, the elements in reported covariance matrix should be generated in the following manner

$$\delta Y_i = \Psi_X(i)\Phi(C)\delta X_i + \Psi(X_i)\Phi_C(C)\delta C \tag{2}$$

$$\sigma_R^2(Y_i) = <(\delta Y_i)^2> = \Psi_X^2(i)\Phi^2(C)\sigma^2(X_i) + \Psi^2(X_i)\Phi_C^2(C)\sigma^2(C) \tag{3}$$

$$\mathrm{Cov}_R(Y_1, Y_2) = <\delta Y_1 \delta Y_2> = \Psi(X_1)\Psi(X_2)\Phi_C^2(C)\sigma^2(C) \tag{4}$$

where

$$\Psi_X(i) = \frac{\partial}{\partial X}\Psi(X_i) \tag{5}$$

$$\Phi_C(C) = \frac{\partial}{\partial C}\Phi(C) \tag{6}$$

Defined $\hat{\Psi}_X(i)$ and $\hat{\Phi}_C(\hat{C})$ by

$$\hat{\Psi}_X(i) = \frac{\partial}{\partial \hat{X}_i}\Psi(\hat{X}_i) \qquad \hat{\Phi}_C(\hat{C}) = \frac{\partial}{\partial \hat{C}}\Phi(\hat{C}) \tag{7}$$

we have

$$\delta Y_i = \hat{\Psi}_X(i)\Phi(\hat{C})\delta X_i + \Psi(\hat{X}_i)\hat{\Phi}_C(\hat{C})\delta C \tag{8}$$

$$\sigma_C^2(Y_i) = \hat{\Psi}_X^2(i)\Phi^2(\hat{C})\sigma^2(X_i) + \Psi^2(\hat{X}_i)\hat{\Phi}_C^2(\hat{C})\sigma^2(C) \tag{9}$$

$$\mathrm{Cov}_C(Y_1, Y_2) = <\delta Y_1 \delta Y_2> = \Psi(\hat{X}_1)\Psi(\hat{X}_2)\hat{\Phi}_C^2(\hat{C})\sigma^2(C) \tag{10}$$

Because the functions Ψ and Φ are unknown, the Eqs. (8) to (10) can not

directly used to obtain corrected values $\sigma_C(Y_i)$ and $\mathrm{Cov}_C(Y_1, Y_2)$. Let us further assume that

$$\Phi(\hat{C}) = \Phi(C) \tag{11}$$

$$\hat{\Phi}_C(\hat{C}) = \Phi_C(C) \tag{12}$$

Due to the same measured C and same relationship for generating Y_1 and Y_2, the assumption of Eqs. (11) and (12) is reasonable. Under this assumption, we have

$$\mathrm{Cov}_C(Y_1, Y_2) = \Psi(\hat{X}_1)\Psi(\hat{X}_2)\hat{\Phi}_C^2(\hat{C})\sigma^2(C) = \frac{\hat{Y}_1\hat{Y}_2}{Y_1 Y_2}\mathrm{Cov}_R(Y_1, Y_2) \tag{13}$$

Then we have

$$\begin{aligned}\sigma_C^2(Y_i) &= \sigma_R^2(Y_i) - \frac{\hat{Y}_i^2}{Y_1 Y_2}\mathrm{Cov}_R(Y_1, Y_2) + \frac{\hat{Y}_i^2}{Y_1 Y_2}\mathrm{Cov}_R(Y_1, Y_2) \\ &= \sigma_R^2(Y_i) + \frac{\mathrm{Cov}_R(Y_1, Y_2)}{Y_1 Y_2}(\hat{Y}_i^2 - Y_i^2)\end{aligned} \tag{14}$$

We call the Eqs. (13) and (14) as Zhao's approximation. If we further assume that

$$\frac{\Psi(X_i)}{\Psi_X(i)} = \frac{\Psi(\hat{X}_i)}{\hat{\Psi}_X(i)} \tag{15}$$

we have

$$\sigma_C^2(Y_i) = \frac{\hat{Y}_i^2}{Y_i^2}\sigma^2(Y_i) \tag{16}$$

The Eqs. (13) and (16) are just Chiba's approximation.

2 Computational Examples

2.1 Data Combination

Assume that Y_1 and Y_2 are two measured data for a same physical quantity <Y>

$$Y_1 = 1.5 \qquad Y_2 = 1.0 \tag{17a}$$

$$\sigma_R^2(Y_1) = 0.1125 \quad \sigma_R^2(Y_2) = 0.05 \quad \mathrm{Cov}_R(Y_1, Y_2) = 0.06 \tag{17b}$$

Usually, evaluators do not know the history obtaining the above data. Combined these two data to obtain the estimate $\hat{Y}$ for <Y> by least square method, we have

$$\text{PPP:} \qquad \hat{Y} = 0.8823 \pm 0.2182$$

If Y_1 and Y_2 were derived from directly measured data by using same function relationship, the above estimate would be incorrect (so–called PPP phenomenon). In this case, the better estimate could be obtained by using approximation methods. The results based on Chiba's and Zhao's approximations are given as follows:

$$\text{Zhao:} \qquad \hat{Y} = 1.1538 \pm 0.2453$$
$$\text{Chiba:} \qquad \hat{Y} = 1.2500 \pm 0.2652$$

Let $C = 1.0 \pm 0.2$, the values of X_i and $\sigma(X_i)$ make Y_i and their covariance matrix equivalent to those in Eq. (17), we have the strict solutions for some given problems:

$$Y = XC: \qquad \hat{Y} = 1.1538 \pm 0.2453$$
$$Y = C / X: \qquad \hat{Y} = 1.3000 \pm 0.2764$$
$$Y = X^2 C: \qquad \hat{Y} = 1.1876 \pm 0.2521$$
$$Y = C / X^2: \qquad \hat{Y} = 1.2627 \pm 0.2680$$

2.2 Curve Fitting

The measured data are given as follows:

X_i	0.8	1.0	2.3	3.4	4.5	7.4	8.8	9.7	(18a)
Y_i	19.	30.	27.	41.	52.	53.	63.	78.	(18b)

$$\sigma_R^2(Y_i) = 0.05 Y_i^2 \quad \mathrm{Cov}_R(Y_i, Y_j) = 0.04 Y_i Y_j \tag{18c}$$

We would like to fit these data by

$$Y(X_i) = \alpha + \beta X_i$$

Directly use the measured data above, we have least square estimates for α and β

$$\text{PPP:} \quad \hat{\alpha} = 10.47 \pm 3.167 \qquad \hat{\beta} = 3.478 \pm 1.002$$

and the fitted curve is obviously wrong (PPP phenomenon, see Fig. 1). The results based on Chiba's and Zhao's approximations are given as follows:

$$\begin{aligned} &\text{Zhao:} \quad \hat{\alpha} = 17.12 \pm 3.819 \quad \hat{\beta} = 5.689 \pm 1.244 \\ &\text{Chiba:} \quad \hat{\alpha} = 18.74 \pm 4.196 \quad \hat{\beta} = 5.669 \pm 1.239 \end{aligned}$$

Also let $C = 1.0 \pm 0.2$, the values of X_i and $\sigma(X_i)$ make Y_i and their covariance matrix equivalent to those in Eq. (18), we have the strict solutions for some given problems:

$$\begin{aligned} &Y = XC: \quad \hat{\alpha} = 17.12 \pm 3.819 \quad \hat{\beta} = 5.689 \pm 1.244 \\ &Y = C / X: \quad \hat{\alpha} = 19.98 \pm 4.440 \quad \hat{\beta} = 5.544 \pm 1.236 \end{aligned}$$

All of the results above are shown in Fig. 1.

3 Conclusion

It is found from the examples that two approximations give better estimates and that Zhao's approximation seems better in the case of increment deriving function and Chiba's better for decrement deriving function.

Acknowledgement

The author would like to thank the Science Foundation of China Nuclear Industry for its support to this work.

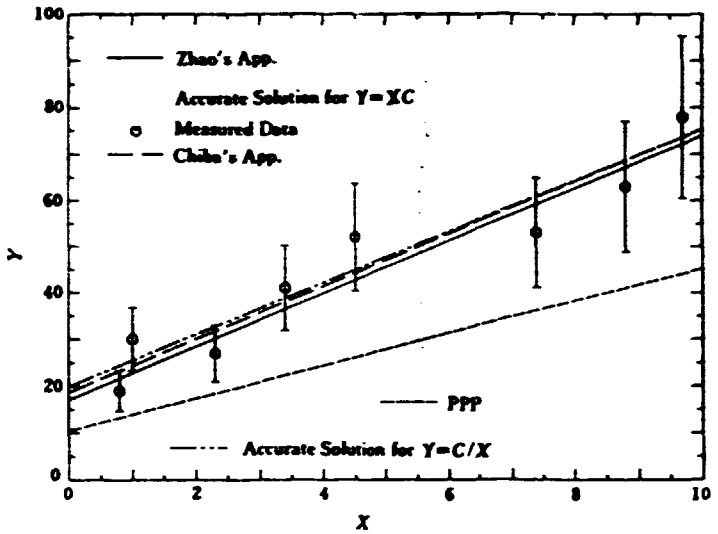

Fig. 1 Comparison of two approximations to deal with PPP

References

[1] Zhao Z., F. G. Perey, "The Covariance Matrix for Derived Quantities and Their Combination", ORNL / TM−12106 (1992)

[2] Zhao Z., F. G. Perey, "Generation of Covariance Matrix for Derived Quantities and Their Least Squares Fitting", "Proc. of Conf. on Evaluation Methodology", BNL (1992)

[3] S. Chiba, D. L. Smith, "Perspectives on PPP and Its Significance in Data Fitting and Evaluation", "Proc. of Conf. on Evaluation Methodology", BNL (1992)

[4] Zhou Delin et al , "Simplified Way to Combine the Correlated Data", CNDP, 5(1991)

CINDA INDEX

Nuclide	Quantity	Energy (eV)		Lab	Type	Documentation			
		Min	Max			Ref	Vol	Page	Date
S	Total	3.50+6	8.00+6	AEP	Eval	Jour CNDP	12	48	Dec 94
K	Total	3.60+5	7.00+6	AEP	Eval	Jour CNDP	12	48	Dec 94
Ti	Total	1.00+5	2.00+7	AEP	Eval	Jour CNDP	12	48	Dec 94
^{59}Co	(n,γ)	1.00+5	3.00+6	ZHN	Theo	Jour CNDP	12	8	Dec 94
Zr	Total	8.40+5	9.30+5	AEP	Eval	Jour CNDP	12	48	Dec 94
^{103}Rh	(n,γ)	1.00+5	3.00+6	ZHN	Theo	Jour CNDP	12	8	Dec 94
Sb	Total	2.50+6	5.00+6	AEP	Eval	Jour CNDP	12	48	Dec 94
Hf	Total	1.50+7	2.00+7	AEP	Eval	Jour CNDP	12	48	Dec 94
Pb	Total	4.70+5	5.00+6	AEP	Eval	Jour CNDP	12	48	Dec 94
	Multiplication	1.35+7	1.49+7	CPC*	Expt	Jour CNDP	12	1	Dec 94
^{197}Au	(n,2n)	Eth	8.00+7	AEP	Eval	Jour CNDP	12	54	Dec 94
^{235}U	Evaluation	1.00+3	2.00+7	AEP	Theo	CNDP	12	14	Dec 94
^{239}Pu	Evaluation	1.00+3	2.00+7	AEP	Theo	CNDP	12	14	Dec 94
^{240}Pu	Evaluation	1.00+3	2.00+7	AEP	Theo	CNDP	12	14	Dec 94

Author, Comments
Liu Tingjin, FOR CENDL-2.1
Liu Tingjin FOR CENDL-2.1
Liu Tingjin, FOR CENDL-2.1
Zhang Xizhi+, SIG, CURV, PREEQ, STATMDL
Liu Tingjin, FOR CENDL-2.1
Zhang Xizhi+, SIG, CURV, PREEQ, STATMDL
Liu Tingjin, FOR CENDL-2.1
Liu Tingjin, FOR CENDL-2.1
Liu Tingjin, FOR CENDL-2.1
Chen Yuan+, TAD, ACTIV
Yu Baosheng+, SIG
Yan Shiwei+, with FUPI
Yan Shiwei+, with FUPI
Yan Shiwei+, with FUPI

* CPC = Southwest Institute of Nuclear Physics and Chemistry, Chengdu, China

(京)新登字 077 号

图书在版编目 (CIP) 数据

核数据进展通讯 (12) = COMMUNICATION OF NUCLEAR DATA PROGRESS NO. 12 : 英文 / 中国核数据中心编. —北京 : 原子能出版社, 1994. 12
ISBN 7-5022-1312-0

I 核 … II. 核 … III. 核能-数据-进展分析-英文 IV. TL-37

中国版本图书馆 CIP 数据核字 (94) 第 13367 号

原子能出版社出版发行
责任编辑 : 李曼莉
社址 : 北京市海淀区阜成路 43 号 邮政编码 : 100037
核科学技术情报研究所印刷
开本 787×1092 1/16 · 印张 8 1/2 · 字数 100 千字
1994 年 12 月北京第一版 · 1994 年 12 月北京第一次印刷

CHINA NUCLEAR SCIENCE & TECHNOLOGY REPOR

ISBN 7-5022-1312-0

9 787502 213121 >

P.O.Box 2103

Beijing, China

China Nuclear Information Centre